NASA CR-134953
R76AEG484

BLADE ROW DYNAMIC DIGITAL COMPRESSOR PROGRAM

VOLUME II

J85 CIRCUMFERENTIAL DISTORTION REDISTRIBUTION MODEL, EFFECT OF STATOR CHARACTERISTICS, AND STAGE CHARACTERISTICS SENSITIVITY STUDY

BY

W.A. TESCH

W.G. STEENKEN

GENERAL ELECTRIC COMPANY
AIRCRAFT ENGINE GROUP

PREPARED FOR

NATIONAL AERONAUTICS AND SPACE ADMINISTRATION

NASA-LEWIS RESEARCH CENTER
CONTRACT NAS3-18526

1. Report No. NASA CR-134953	2. Government Accession No.	3. Recipient's Catalog No.
4. Title and Subtitle Blade Row Dynamic Digital Compression Program Volume II J85 Circumferential Distortion Redistribution Model, Effect of Stator Characteristics, and Stage Characteristics Sensitivity Study.		5. Report Date July 1978 6. Performing Organization Code
7. Author(s) W.A. Tesch W.G. Steenken		8. Performing Organization Report No. R76AEG484 10. Work Unit No.
9. Performing Organization Name and Address General Electric Company Aircraft Engine Group Cincinnati, Ohio 45215		11. Contract or Grant No. NAS3-18526 13. Type of Report and Period Covered Contractor Report
12. Sponsoring Agency Name and Address National Aeronautics and Space Administration Washington, D.C. 20546		14. Sponsoring Agency Code

15. Supplementary Notes

Project Monitors: D.G. Evans, P.G. Batterton and E.J. Graber, Jr.
NASA-Lewis Research Center, Cleveland, Ohio 44135

16. Abstract

This report presents the results of dynamic digital blade row compressor model studies of a J85-13 engine. The initial portion of the study was concerned with the calculation of the circumferential redistribution effects in the blade-free volumes forward and aft of the compression component. Although blade-free redistribution effects were estimated, no significant improvement over the parallel-compressor type solution in the prediction of total-pressure inlet distortion stability limit was obtained for the J85-13 engine. Further analysis was directed to identifying the rotor dynamic response to spatial circumferential distortion. Inclusion of the rotor dynamic response led to a considerable gain in the ability of the model to match the test data. The impact of variable stator loss on the prediction of the stability limit was evaluated. An assessment of measurement error on the derivation of the stage characteristics and predicted stability limit of the compressor was also performed.

17. Key Words (Suggested by Author(s))	18. Distribution Statement
Compressor Stability Blade Row Model Parallel Compressor Model Flow Redistribution	

19. Security Classif. (of this report)	20. Security Classif. (of this page)	21. No. of Pages	22. Price*
Unclassified	Unclassified		

*For sale by the National Technical Information Service, Springfield, Virginia 22151

FOREWORD

The program described in this report was conducted by the Aircraft Engine Group of the General Electric Company, Cincinnati, Ohio for the NASA Lewis Research Center, National Aeronautics and Space Administration under contract NAS3-18526.

The program was carried out under the technical cognizance of Mr. D.G. Evans, Mr. P.G. Batterton and Mr. E.J. Graber, Jr. of the NASA Lewis Research Center Engine Research Branch.

The contract effort was conducted at the Evendale Plant of the Aircraft Engine Group, Cincinnati, Ohio under the technical direction of Dr. W.G. Steenken with Mr. W.A. Tesch being the prime technical contributor. Support was provided by Mrs. V.A. Haywood of the Lynn Plant, Aircraft Engine Group, Lynn, Massachusetts in deriving the stage characteristics with the inclusion of stator losses and by Miss. S.I. Santel in preparing this report for publication.

TABLE OF CONTENTS

LIST OF ILLUSTRATIONS

LIST OF ILLUSTRATIONS (Continued)

LIST OF ILLUSTRATIONS (Concluded)

LIST OF ILLUSTRATIONS (Concluded)

LIST OF TABLES

NOMENCLATURE

A	-	Area or Constant
ALF	-	Aft Looking Forward
C_z	-	Axial Velocity
C_u	-	Absolute Tangential Velocity
F_B	-	Blade Force
L	-	Volume Length
IGV	-	Inlet Guide Vane
N	-	Rotor Speed in Revolutions per Minute
P	-	Static Pressure
P_M	-	Mean Static Pressure
P_T	-	Total Pressure
R	-	Specific Gas Constant
S_F	-	Entropy Production Term
T_T	-	Total Temperature
U	-	Pitch Line Wheel Speed
V	-	Volume
W_z	-	Axial Flow Rate
W_θ	-	Tangential Flow Rate
W'	-	Relative Velocity
c	-	Blade Chord
g_o	-	Gravitational Constant
i	-	Incidence Angle
i_e	-	Effective Incidence Angle
i_i	-	Instantaneous Incidence Angle
i_o	-	Mean Incidence Angle
r	-	Pitch-line Radius
s	-	Specific Entropy
t	-	Time
α	-	Absolute Air Angle
γ	-	Ratio of Specific Heats
δ	-	Deviation Angle or P_T/P_{STD}

NOMENCLATURE (Concluded)

θ	-	T_T/T_{STD}
ξ	-	Dummy Variable
ρ	-	Density
τ	-	Time Constant
$\bar{\omega}$	-	Total-Pressure Loss Coefficient
ϕ	-	Flow Coefficient $\left(\frac{C_{z_i}}{2\pi N r_i}\right)$
Ψ	-	Work Coefficient $\frac{\frac{\gamma}{\gamma-1} g_o R \left(T_{T_{i+1}} - T_{T_i}\right)}{[2\pi N(r_i)]^2/2}$
ψ'	-	Pressure Coefficient $\frac{\frac{\gamma}{\gamma-1} g_o R T_{T_i} \left[\left(\frac{P_{T_{i+1}}}{P_{T_i}}\right)^{(\gamma-1)/\gamma} - 1\right]}{[2\pi N(r_i)]^2/2}$

SUBSCRIPTS

2	-	Compressor Entrance Station
3	-	Compressor Discharge Station
M	-	Mean
T	-	Total
i	-	i-th Station
j	-	j-th Tangential Face
k	-	k-th Volume
z	-	Axial Direction
θ	-	Tangential Direction

SUPERSCRIPTS

$\overline{\quad\quad}$	-	Volume Average (Clean or Distorted Sector)
$'$	-	Relative Frame of Reference

1.0 SUMMARY

The objectives of this study were to investigate potential techniques for improving the stability modeling of clean-inlet and distorted-inlet flows and to evaluate the sensitivity of stage characteristics to measurement error. The analyses were verified by comparison with the clean-inlet performance and the 1/rev circumferential total-pressure distortion performance of a J85-13 engine tested at NASA Lewis Research Center. The calculation of 1/rev distorted flow circumferential redistribution effects in the blade-free volumes of the compression component was investigated. This was accomplished through the addition of the angular momentum equation and the inclusion of the tangential flow terms to the equations of continuity, axial momentum, and energy. Analysis of the total-pressure distortion simulations showed that it was possible to calculate redistribution effects in blade-free volumes using a coarse grid in conjunction with a lumped volume technique. The technique is numerically stable, but is not adequate for defining the fine details of flow fields. However, the technique does meet the intended purpose of coupling with the parallel-compressor model and providing volume averaged redistribution effects as compressor sector entrance flow conditions. Examination of the compression-component performance indicated no significant improvement over the parallel-compressor-type solution in predicting the stability limit. This finding is probably the result of the manner in which the inlet guide vanes are modeled and the fact that the presence of high-solidity inlet guide vanes minimize the effects of tangential flow redistribution. It is anticipated that the inclusion of the effects of redistribution will probably have a more significant effect when coupled with compressor models not possessing inlet guide vanes.

The aerodynamic response of a blade row passing through a distorted flow region was modified using a simple differential form of the dynamic response. Significant gains in the ability to match the distorted inlet compressor performance were made although stage mismatching poses some limitations to the technique.

Analyses conducted heretofore have been performed with the constraint that all losses are assigned to the rotor of a stage, while the stator is considered lossless. A study was conducted in which variable stator losses were derived and their impact on the predicted stability limit and on the location of the stalling stage was assessed. It was concluded that the dynamic model was more sensitive to the throttling process with the inclusion of variable stator losses, although no significant change in the overall compressor stability was observed.

Finally, studies were conducted in which the sensitivity of the stage characteristics to measurement error was evaluated. The total pressure of one stage was varied one percent while the overall compressor characteristic was maintained. Clean-inlet-throttling simulations were then conducted in order to determine the impact on the predicted stability limit. These computations indicated that no significant change occurred in the prediction of the stability limit or the stalling stage location.

2.0 INTRODUCTION

Analysis of the results obtained from the General Electric Dynamic Digital Blade Row Compression Component Stability Model during clean-inlet-flow and distorted-inlet-flow studies of the J85-13 turbojet engine (Reference 1) identified three areas needing study. These areas were:

1. Effect of upstream redistribution of circumferentially distorted inlet flows on surge line predictions.

2. Effect of including stator losses on stability predictions.

3. Effect of measurement inaccuracies on derived stage characteristics.

During the first year of this two year effort, the Dynamic Digital Blade Row Compression Component Stability Model was modified to a multi-sector parallel compressor configuration to permit simulation of inlet flows with 180°, 1/rev total-pressure, total-temperature, and combined total-pressure and total-temperature distortions. The inlet total pressure and total temperature were specified for each sector and all sectors exited to a uniform static pressure downstream of the compressor discharge diffuser. Throttling was accomplished by ramping the flow function at a plane simulating the turbine diaphragm. Surge was predicted when one sector encountered the clean inlet surge line and developed an aerodynamic instability while operating on its clean-inlet-flow speed-line characteristics. As with most parallel-compressor models, the loss in surge pressure ratio is more accurately predicted when the speed lines are steep than when the speed lines have low slopes. Because of the low gap-to-radius ratios that are characteristic of the J85-13, it was contended that this overprediction of loss in surge pressure ratio could not be attributed to internal crossflows between the distorted and undistorted sectors. This contention is supported by the analytical work of Plourde and Stenning (Reference 2) who showed that for the gap-to-radius ratios characteristic of modern compressors, very little crossflow occurred. Spring (Reference 3), using the technique of Plourde and Stenning, predicted the redistribution effect of a compressor on an upstream distorted flow. It was found that for a flow exiting from a screen far upstream of a compressor, the imposed total-pressure distortion with its attendant uniform static pressure and large flow differences was transformed at the compressor face to a flow with essentially its total-pressure distortion unchanged. However, static-pressure and circumferential-velocity distortions were created while the flow distortion tended to a more uniform distribution. Further, the effect of internal crossflows were examined in a recent study by Tesch, Moszee, and Steenken (Reference 4). They concluded that including crossflow in the model did not improve the predicted results.

Analysis of all these results led to the conclusion that the upstream boundary conditions imposed upon a parallel compressor model are unrealistic. During the course of the effort reported upon herein, the upstream flow field was modeled by including the angular momentum macrobalance and by including

the tangential flow contributions to the mass and energy macrobalances. It was felt that use of a coarse grid (same number of circumferential sectors as used in the parallel compressor) would be sufficient to establish the gross characteristics of the flow field and yet would give a sufficiently accurate estimate of the flow field entering the compressor IGV's for the purposes of compression component stability computations. Hence, the upstream boundary conditions were imposed upstream at the plane of the screen and the flow field was allowed to adjust to the more uniform volumetric flow per unit area distribution that is demanded by the pumping characteristics of the compressor. Further, the model was structured in such a way that circumferential redistribution could be included in the free volume located between the trailing edge of the IGV and the leading edge of rotor 1 and in the free volumes between the compressor discharge and the choke plane located at the simulated turbine diaphragm location if desired.

Verification of the effect of circumferential flow redistribution in the presence of circumferential distortion was accomplished by simulating 180- and 60-degree extent 1/rev total-pressure distortion patterns and comparing these results with test results in terms of pressure ratio and flow at surge for at least two corrected speeds.

A second topic of distortion analysis modeling to be investigated was that of rotor dynamic response. Since rotor blade rows cannot respond instantaneously to changes in inlet conditions when passing through a distorted flow field, a preliminary formulation of a rotor dynamic response function was developed. The response function was evaluated through the analysis of circumferential inlet total-pressure distortions of varying extents at several different corrected speeds.

All total-pressure losses were assumed to occur only in rotor blade rows during the Reference 1 study. This assumption is often used when interstage data are limited and is not a limitation of the blade row model per se. The effect of this assumption on surge line predictions and the location of the stage initiating the instability, were evaluated by estimating stator blade-row losses and including them in the model. Then assuming that the stage characteristics remained unchanged, new relative total-pressure loss coefficients and rotor deviation angles were derived for each rotor. The improvements offered in the prediction of the loss of surge pressure ratio by including stator losses in the model were evaluated by throttling clean-inlet flows to instability. The resulting loss in surge pressure ratios and corrected flows at surge were compared with test data. Further, the stage where instability was initiated with clean inlet flow was compared with the Reference 1 results.

During analysis of test data to establish stage characteristics during the Reference 1 study, it was found that the stage characteristics based upon data (and assumptions required in lieu of missing test data) when stacked, did not properly simulate the overall speed line. This was due to some stages being loaded differently than design goals or experience would dictate. Although, the reason for this discrepancy was not ferretted out, the possibility of instrumentation or instrumentation-induced errors could never

be ruled out. Since the Dynamic Digital Blade Row Compression Component Stability Model requires loss coefficients and deviation angles, which are derived from stage characteristics as input, it was deemed appropriate to determine the manner in which changes in stage characteristic levels would effect stability predictions.

This effort was conducted by parametrically varying the pressure coefficient of one stage and maintaining the overall pressure ratio - corrected flow characteristic of the speed line. The model was then throttled with clean inlet flow to surge and the difference in surge pressure ratio and location of the stage initiating instability noted.

3.0 BLADE ROW DYNAMIC MODEL WITH CIRCUMFERENTIAL REDISTRIBUTION

The parallel-compressor analyses of circumferential inlet distortion reported upon in Reference 1 revealed certain areas in which an improvement in the technique of surge line prediction was suggested, particularly in the low speed regime. This section reports upon an investigation in which the parallel-compressor Dynamic Digital Blade Row Compression Component Stability Model was modified to account for the circumferential redistribution effects experienced with circumferentially distorted inlet flows. These modifications permit the model to calculate the circumferential readjustment of flow in blade-free volumes upstream and downstream of the compression component. Evaluation of the model results was accomplished through the analysis of circumferential total-pressure distortion on the "Moss" J85-13 engine (Reference 5). A description of the J85-13 and the basic model geometry may be found in Reference 1.

The model geometry as reported in Reference 1 was modified slightly for the redistribution modeling activities. The modifications consisted of the addition of five additional blade-free volumes to the front of the model. These volumes and the two original blade-free volumes upstream of the inlet guide vanes were added to permit calculation of flow redistribution in the region between the distortion screen and the inlet guide vanes and to maintain volume lengths no longer than the longest compressor blade row. Figure 1 provides a schematic of the model geometry used in the redistribution analyses and Table 1 provides a tabulation of the additional geometric lengths and areas.

3.1 REDISTRIBUTION ANALYTICAL TECHNIQUE

3.1.1 Equations of Change

The complete set of non-linear partial differential equations which describe the transfer and storage of mass, momentum, and energy within a fluid are called the equations of change (Reference 6). These equations have been integrated once over an arbitrary volume of the flow system to obtain the macroscopic balances for quasi two-dimensional flow without heat transfer and internal fluid shear and are reproduced below in the form in which they are used in the dynamic compression component model.

$$\frac{\partial \bar{c}_k}{\partial t} = \frac{1}{V_k}\left[W_{z_i} - W_{z_{i-1}} + \left|W_{\theta_j} - W_{\theta_{j-1}}\right|\right] \tag{1}$$

$$\frac{\partial \bar{W}_{z_k}}{\partial t} = \frac{g_o}{L_z}\left[\frac{W_{z_i} C_{z_i}}{g_o} - \frac{W_{z_{i-1}} C_{z_{i-1}}}{g_o} + \left|\frac{W_{\theta_j} C_{z_j}}{g_o} - \frac{W_{\theta_{j-1}} C_{z_{j-1}}}{g_o}\right|\right.$$

$$\left. + P_i A_i - P_{i-1} A_{i-1} - P_M(A_i - A_{i-1}) + F_B\right] \tag{2}$$

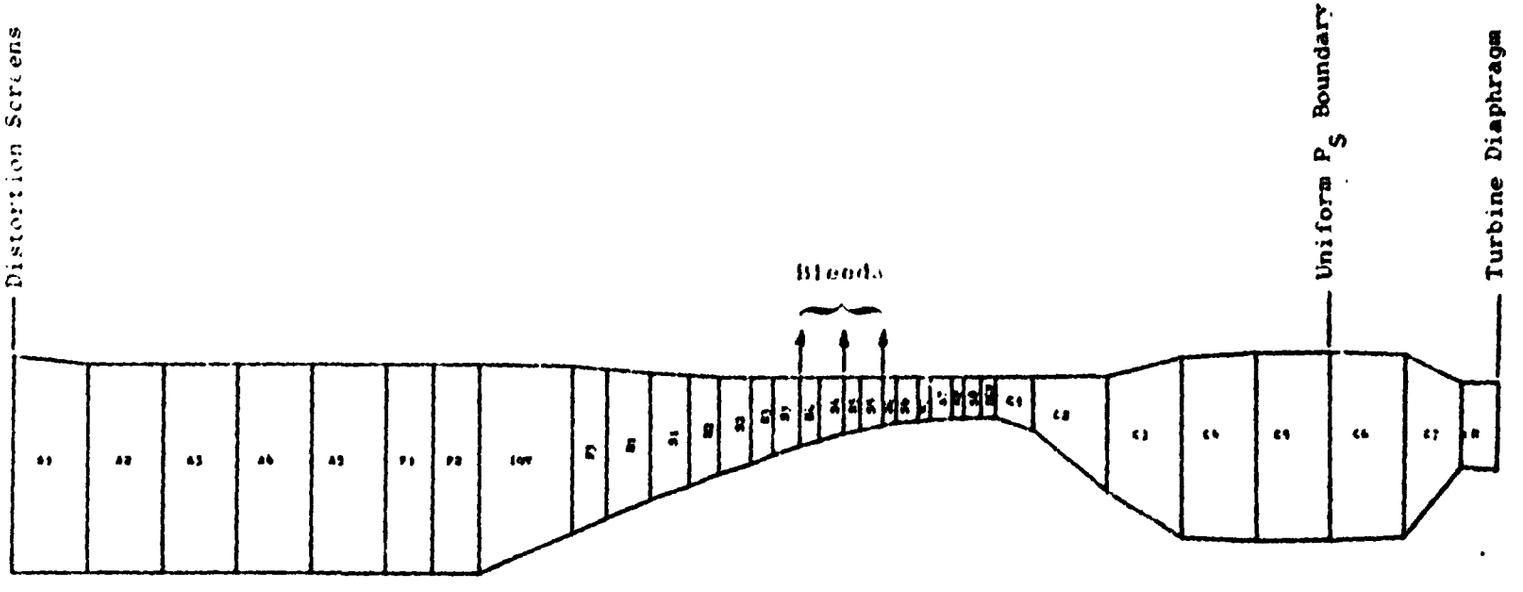

Figure 1. Schematic Of Model Volumes.

Table 1. 185-13 Compressor Model Additional Volume Geometry.

$$\frac{\partial \bar{W}_{\theta_k}}{\partial t} = \frac{g_o}{\bar{r}L_\theta}\left[\frac{r_i W_{z_i} C_{u_i}}{g_o} - \frac{r_{i+1} W_{z_{i+1}} C_{u_{i+1}}}{g_o} - \frac{r_j W_{\theta_j} C_{u_j}}{g_o} - \frac{r_{j+1} W_{\theta_{j+1}} C_{u_{j+1}}}{g_o} + \bar{r}(P_j - P_{j-1})A_j\right] \quad (3)$$

$$\frac{\partial \overline{\rho s}_k}{\partial t} = \frac{1}{V_k}\left[W_{z_i} S_i - W_{z_{i+1}} S_{i+1} + \{W_{\theta_j} S_j - W_{\theta_{j+1}} S_{j+1}\} + S_F\right] \quad (4)$$

The terms enclosed by braces, { }, in the above equations are additions to the one-dimensional forms of the continuity, axial momentum and energy equations as specified in Reference 1. Equation 3 is the macro-balance expression for the conservation of angular momentum. Subscripted variables on the right-hand side of the equations refer to quantities at the faces of the control volume; i.e., "i" refers to the axial faces and "j" refers to the tangential faces. Variables on the left-hand side refer to volume averaged quantities, i.e., in generalized form

$$\bar{\xi} = \frac{\int \xi \, d\,V}{\int d\,V} \quad (5)$$

The energy equation (Equation 4) was derived by combining the equation of change for energy and one of the thermodynamic TdS relationships. These equations were used in this form for calculating the volume averaged quantities in each sector in blade-free volumes. The equations were used without the terms enclosed by braces and without Equation 3 for bladed volumes.

3.1.2 Force, Pressure, and Entropy Production Terms

This set of equations (other than being applicable to quasi two-dimensional flows without heat transfer, without internal fluid shear, and a finite, but small volume) describes the state of a fluid in motion. In order for a solution to be obtained, it is necessary to supply the caloric and thermal equations of state and expressions for F_B, P_M, and S_F. F_B (Equation 2) represents the blade force acting upon the fluid and includes contributions from the energy-producing torque term and the drag force term. P_M (Equation 2) represents the mean pressure over the lateral surface area of the volume

element and is sometimes referred to as the drum and shroud force. It is calculated from a linear combination of the entrance and exit axial static pressures. S_F (Equation 4) is the term which represents the total rate of irreversible conversion of mechanical to internal energy and, in the case of this model, represents the entropy production due to blade row losses. Details of the derivations of these three terms may be found in Reference 1.

3.1.3 Calculation Technique

Time-dependent solution of the system of equations (Equations 1 through 4 and expressions for F_B, P_M and S_F) that comprise the dynamic digital compression component model is effected through a Taylor series which establishes the values of the four independent volume-averaged variables ($\bar{\rho}$, $\bar{W}_z$, $\bar{W}_\theta$, $\overline{\rho s}$) at the next increment in time. This technique is identical to that discussed in Reference 1 with the addition that the tangential terms also must be considered, that is, just as there are axial stations, there are circumferential stations. The circumferential station values are obtained using an interpolation technique which weights the adjacent volume-averaged quantities in a manner inversely proportional to their respective volumes. Hence, the station values of density ρ_i, circumferential flow $W_{\theta i}$, axial velocity C_{z_i}, and tangential velocity C_{θ_i} are obtained according to the generalized relationship

$$\xi_i = \frac{\bar{\xi}_k V_{k-1} + \bar{\xi}_{k-1} V_k}{V_{k-1} + V_k} \tag{6}$$

Equation (6) maximizes the effect of the small extent sector which is in keeping with the fact that the sector station is closer to the center of the smaller volume than it is to the center of the larger volume. Thus, the station value is more likely to be closer to the small sector-volume averaged value than it is to the large sector-volume averaged value. Further details on the Taylor series prediction of volume-averaged variables are given in Reference 1.

The redistribution model was developed as an extension of the Dynamic Digital Blade Row Compression Component Stability Model discussed in Reference 1 and as such the computational technique is quite similar to that illustrated in Figure 12 of that document. The significant difference between the two techniques is the addition of a sector calculation loop inside the volume calculation loop for the redistribution model.

3.2 INITIALIZATION

Like all time-dependent solutions, the dynamic redistribution model requires a set of initial conditions in order that the transient event may be simulated. However, in the case of the circumferential redistribution analysis, the problem of initializing a transient event is complicated by the fact that

there is no easily obtainable steady-stage solution as there is for axisymmetric flow. Therefore the starting conditions for the transient simulation were obtained by allowing a steady-state parallel-compressor solution to settle out under the constraint of a constant exit-flow function. Thus, the model uses a time-dependent calculation until the flow derivatives are small enough to insure that the flow has readjusted to a valid set of initial conditions for the transient event simulation.

3.3 CIRCUMFERENTIAL REDISTRIBUTION DISTORTION ANALYSIS

The effect of circumferential (tangential) flow redistribution on the prediction of the behavior of the distorted surge line was evaluated through the simulation of 60° and 180° extent 1/rev circumferential inlet total-pressure distortions at 80% and 100% corrected speeds. The distortions were produced by a screen with 49% blockage and were tested on the "Moss" J85-13 engine as reported in Reference 5. The model was constructed such that redistribution was allowed in the seven blade-free volumes upstream of the IGV and in the blade-free volumes between the OGV and the uniform static-pressure boundary condition (see Figure 1).

The dynamic redistribution model was used to investigate a 180°, 1/rev circumferential total-pressure distortion at 80% corrected speed. The model was subdivided circumferentially into six 60° sectors, three each in the clean-inlet and the distorted-inlet regions of the flow. The resultant operating points of the individual sectors after allowing settling out for 800 time-steps from the initial parallel-compressor solution are shown in Figure 2. The operation of each sector differs little from the original operating points of the sectors of the parallel-compressor case. It should be noted that Figure 2 represents the performance as defined by the region from the IGV leading edge to the OGV trailing edge and does not illustrate the readjustment of the flow upstream and downstream of the compressor in the blade free volumes. Figures 3 and 4 illustrate the axial flow distribution and flow angle distributions in the blade free volumes. The increase of axial flow in the distorted inlet flow sectors can be observed (Figure 3) with increasing distance downstream of the distortion screen. This influx of flow into the distorted sectors is further substantiated by the flow angle distribution (Figure 4). As one might intuitively expect, the fluid tends to flow into the distorted (low total pressure) flow sectors downstream of the distortion screen. Figures 3 and 4 also illustrate the downstream readjustment of the flow between the OGV and the uniform static-pressure boundary condition. Figure 5 illustrates the tangential-flow distribution in the blade-free volumes upstream and downstream of the compressor.

At 60°, 1/rev circumferential total-pressure distortion also was investigated at 80% corrected speed. Again the flow-field was divided into six 60° sectors with total-pressure distortion occuring only in one of the sectors. The operating points of the sectors after settling out from the parallel-compressor initialization are shown in Figure 6. In addition, a throttling simulation was performed. Little difference between the parallel-compressor and redistribution stability limits was noted. The axial flow, flow angle, and tangential flow distributions in the blade-free volumes are given in Figures 7, 8, and 9.

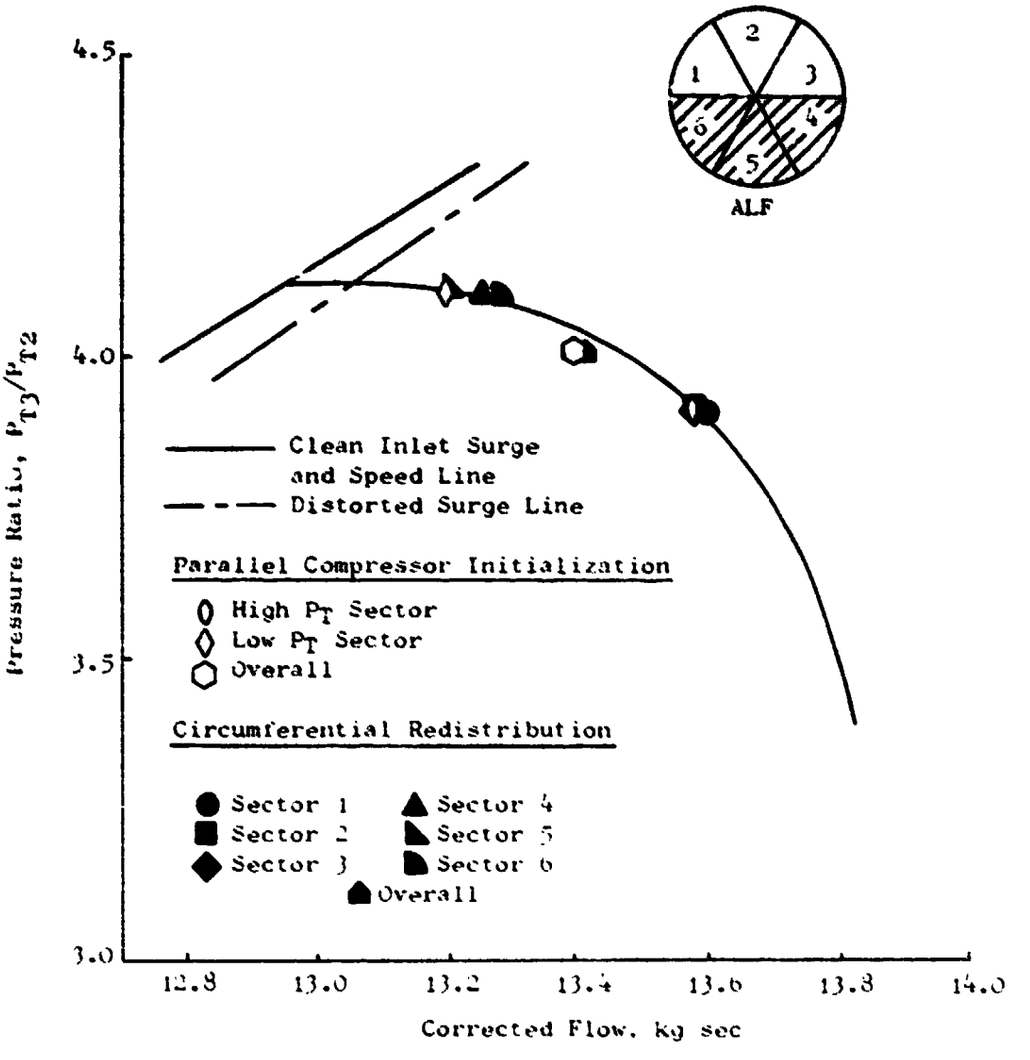

Figure 2. Circumferential Redistribution Analysis of "Moss" J85-13 Engine with 180°, 1 rev Total-Pressure Distortion, 80% $N_1\sqrt{\theta}$ - Sector Performance.

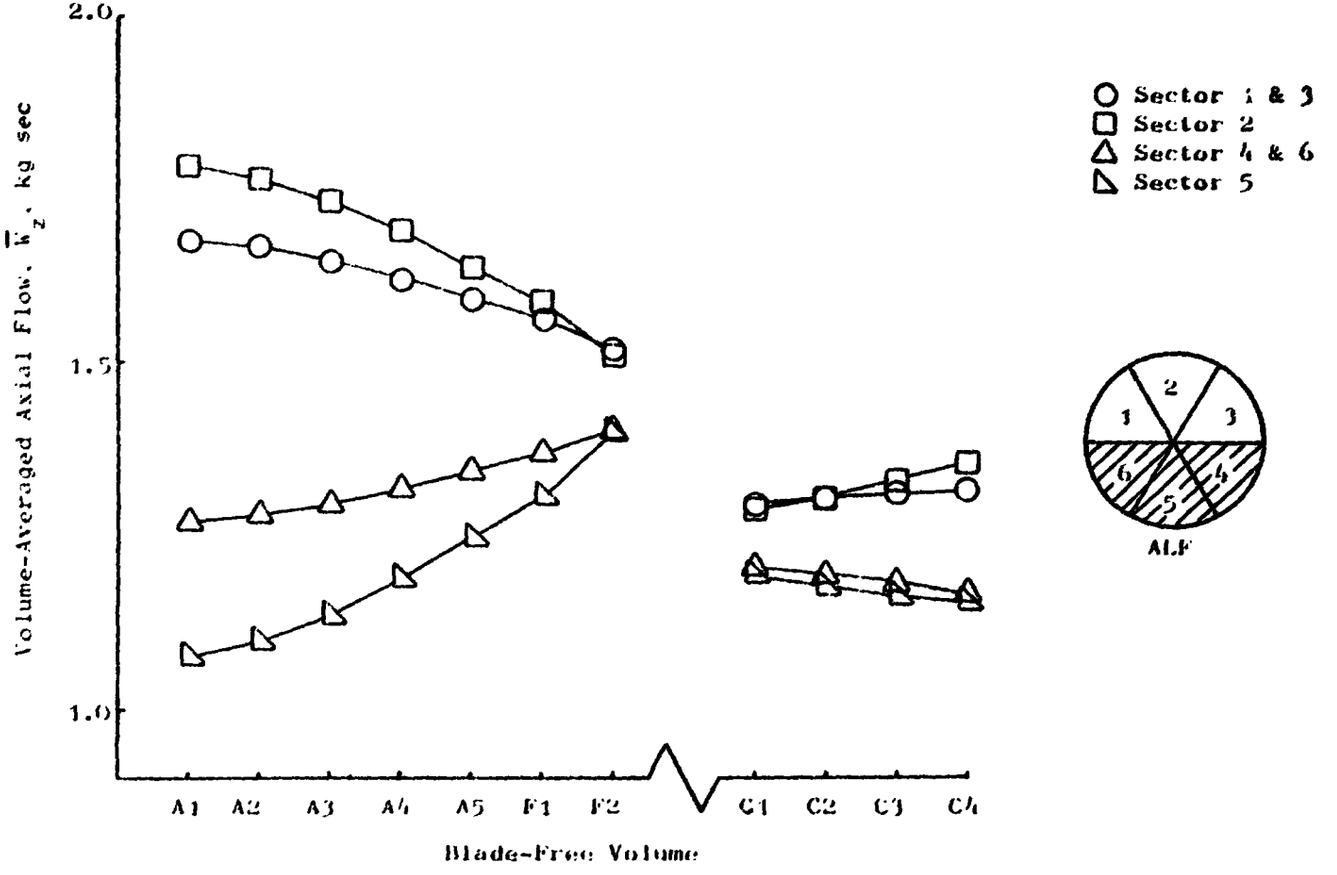

Figure 3. Circumferential Redistribution Analysis of "Moss" J85-13 Engine With 180°, 1/rev Total-Pressure Distortion, 80% $N/\sqrt{\theta}$ - Axial Flow Distribution.

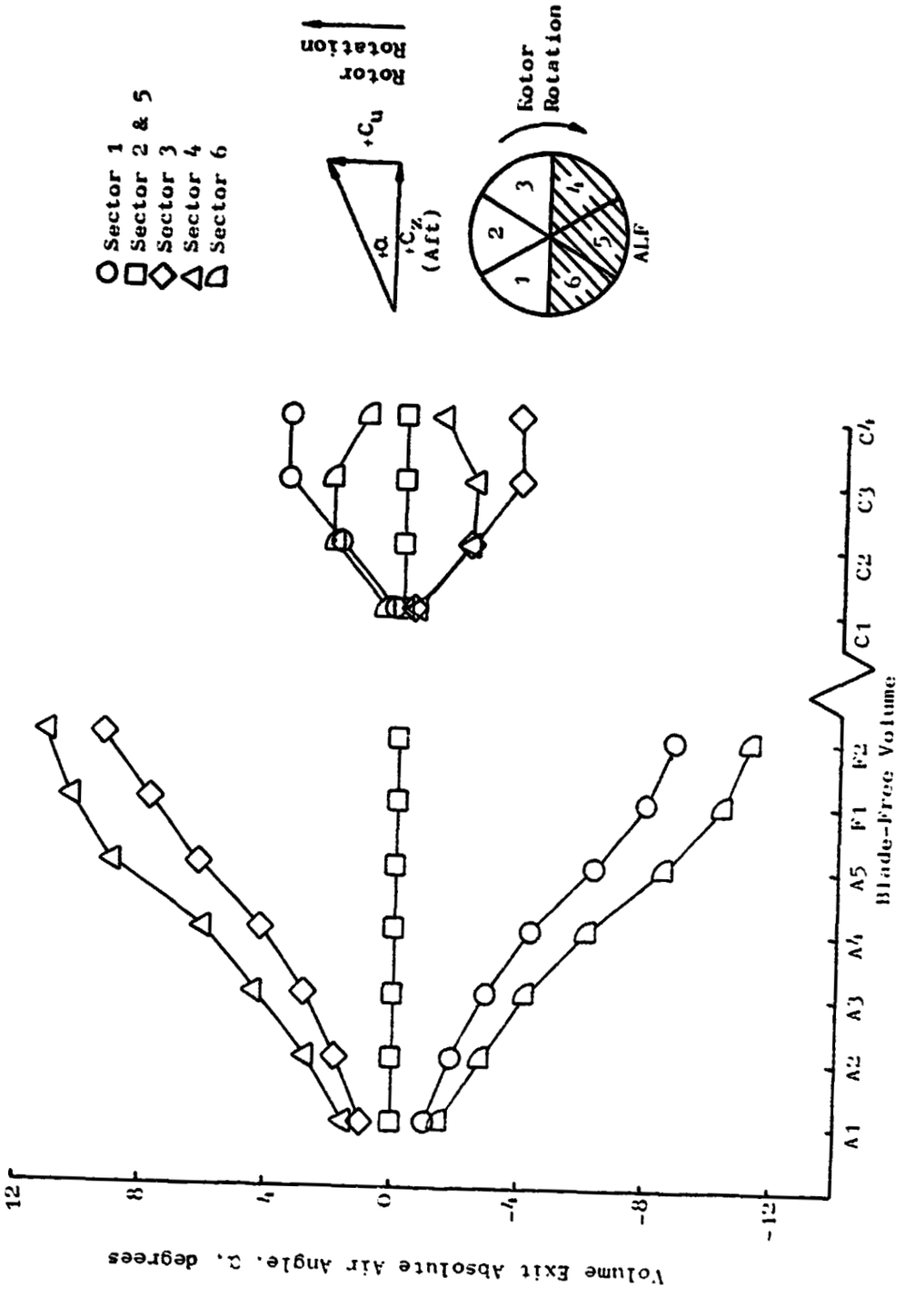

Figure 4. Circumferential Redistribution Analysis of "Moss" J85-13 Engine With 180°, 1/rev Total-Pressure Distortion, 80% $N/\sqrt{\theta}$ - Flow Angle Distribution.

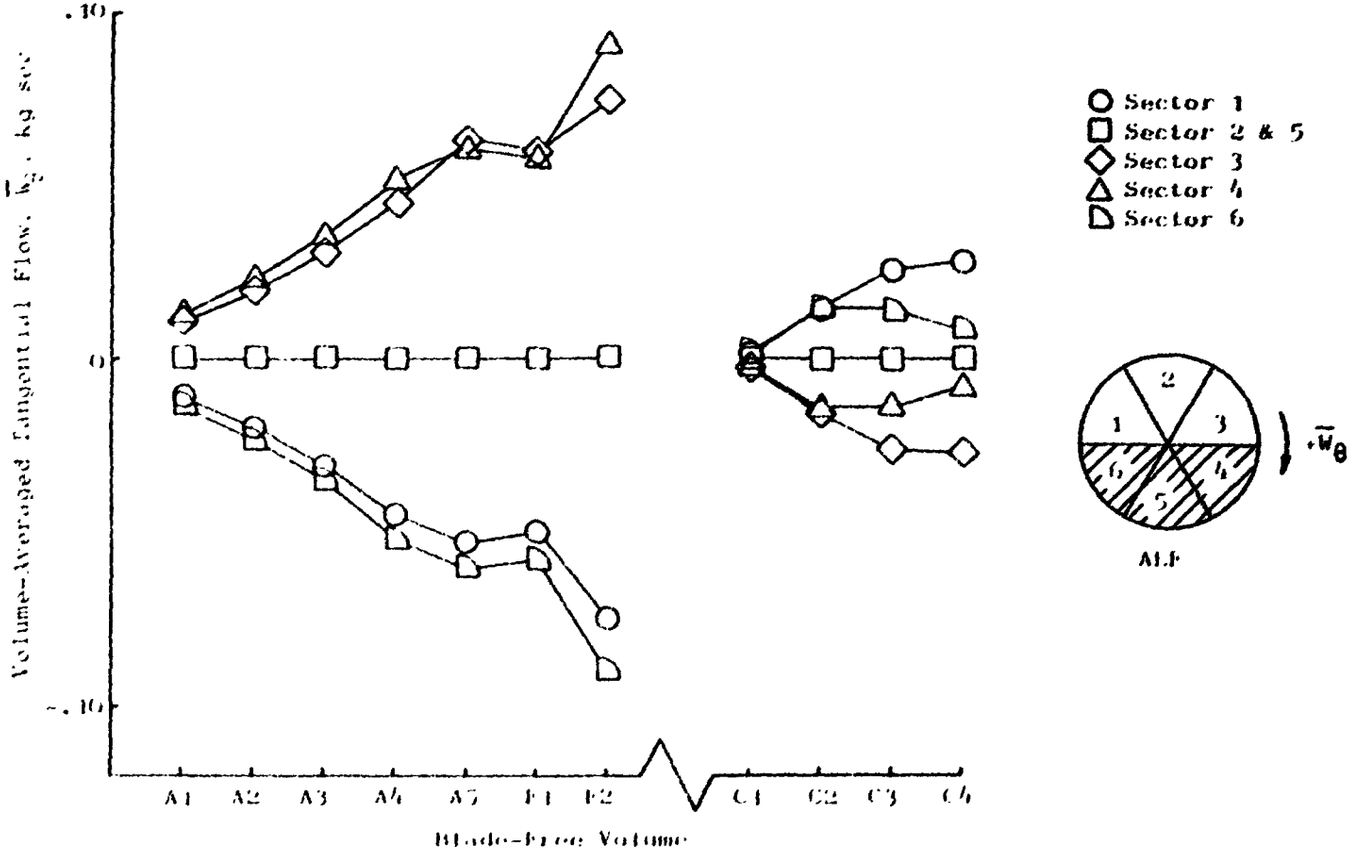

Figure 7. Circumferential Redistribution Analysis of "Mass" J85-13 Engine With 180°, 1/rev Total-Pressure Distortion, 80% $N/\sqrt{\theta}$ - Tangential Flow Distribution.

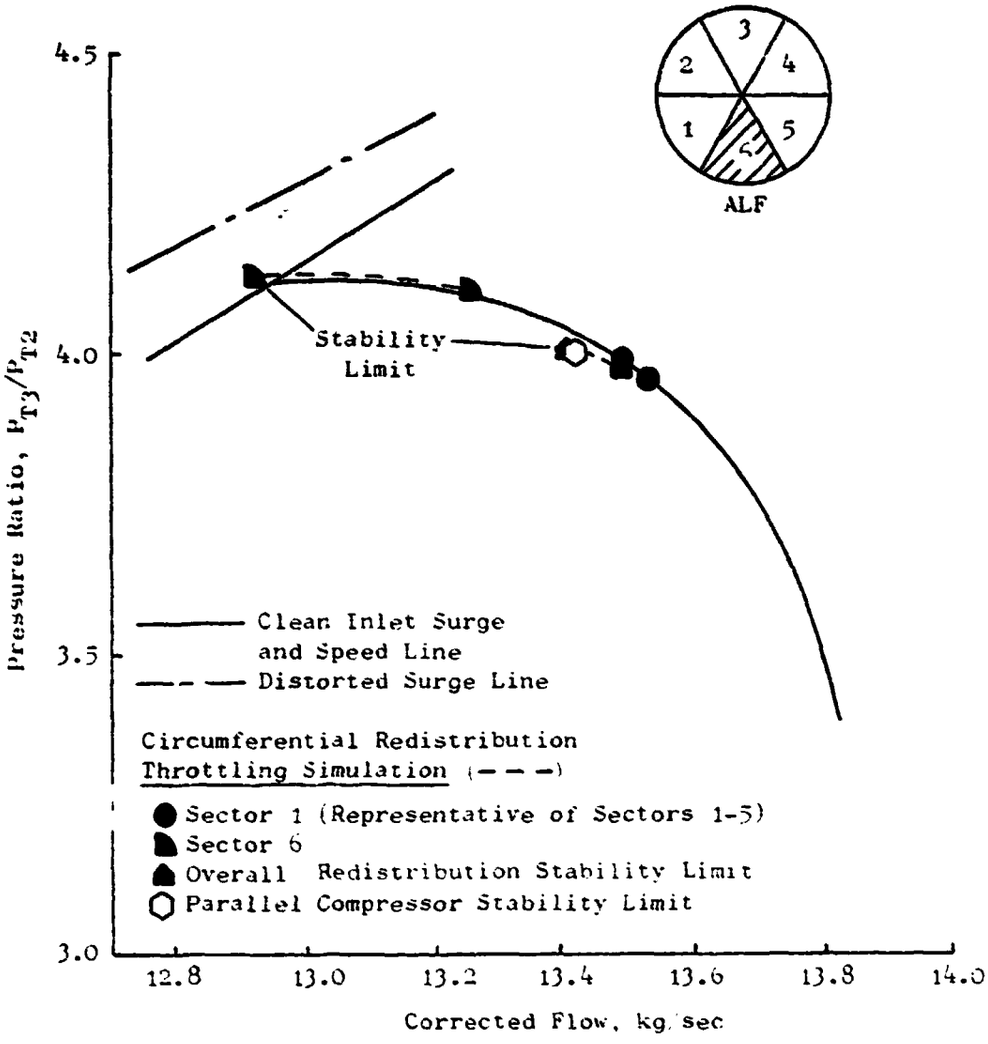

Figure 6. Circumferential Redistribution Analysis of "Moss" J85-13 Engine With 60°, 1/rev Total-Pressure Distortion, 80% $N/\sqrt{\theta}$ - Sector Performance.

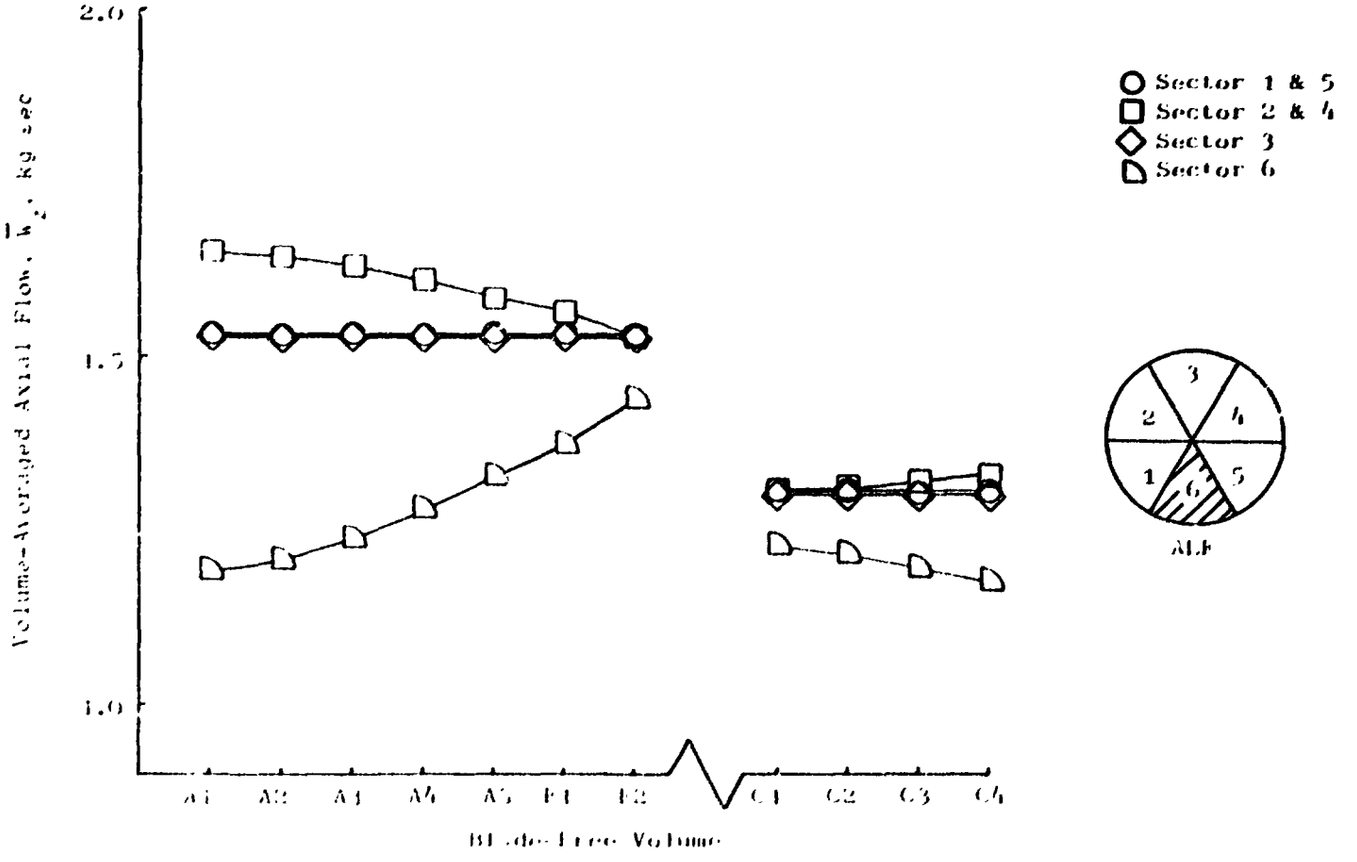

Figure 7. Circumferential Redistribution Analysis of "Mo " 185-13 Engine With 60°, 1/rev Total Pressure Distortion, 80% N/$\sqrt{\theta}$ - Axial Flow Distribution.

ORIGINAL PAGE IS
OF POOR QUALITY

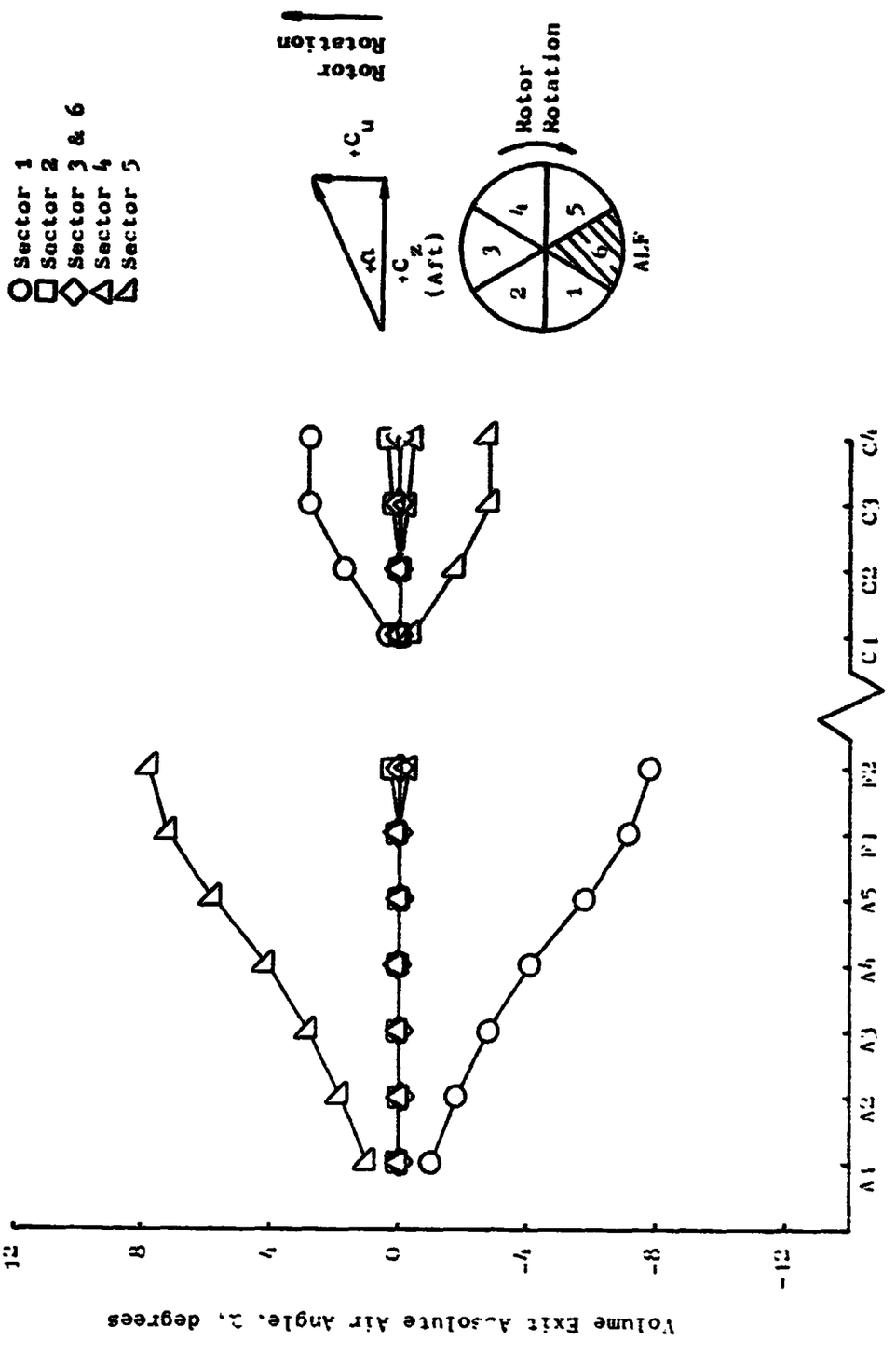

Figure 8. Circumferential Redistribution Analysis of "Moss" J85-13 Engine With 60°, 1/rev Total-Pressure Distortion, 80% N/√θ - Flow Angle Distribution.

Figure 9. Circumferential Radial Distribution Analysis of "Mass" JT8-13 Engine With 60°, 1/rev Total-Pressure Distortion, 85% $N/\sqrt{\theta}$ - Tangential Flow Distribution.

Due to the symmetry of forces on Sector 3 (the clean-inlet-flow sector opposite the distorted sector) very little change is seen in the axial flow, tangential flow, and flow angle from the distortion screen to the compressor face. These results are supported by the Reference 7 component tests, during which detailed flow surveys were taken at the compressor inlet when operating with distorted inlet flow conditions. These tests showed that the region opposite the screen possessed almost no circumferential variation in axial velocity or flow angle. Examination of Figures 7 and 9 reveals two interesting facts which are not consistent with intuition: 1) the increase in flow in the distorted sector is due to a decrease in axial flow in Sectors 2 and 4 (sectors which are not adjacent to the distorted sector) and 2) there is a net tangential flow only in the two Sectors (1 and 5) adjacent to the distorted sector. In an attempt to obtain a better understanding of this predicted flow process, the circumferential static-pressure distribution was examined. This was accomplished by plotting the volume exit static pressure* (a primary flow variable) at each axial station as a function of angular position (Figure 10). The important feature of this plot is that "side lobes" of low static-pressure are being developed where it would be anticipated that no static-pressure deficit would occur although they have disappeared by the time the IGV's are reached. In order to determine what effect interpolation in the circumferential direction played, the interface static-pressures between sectors were plotted (Figure 11). This plot shows a better behaved distribution (no side lobes), but the static-pressure distortion has been spread over 120° with a reduced minimum magnitude. It is well recognized that some of these flow field calculation anomolies can be removed by going to a differential formulation as opposed to the integral formulation that is being used. However, such a formulation would not match well with the integral compressor formulation which we wished to maintain. While it would be quite satisfying if the integral flow field solution gave an adequate representation of the complete flow field in blade free volumes, it is important to realize that the major objective of the integral circumferential flow redistribution formulation is to provide a better representation of the flow entering the compression component and not necessarily of the whole flow field. At this point, it was appropriate to investigate the cause of this behavior noting that it also occurs in other flow variables. The effects of the following items were investigated:

a) A finer circumferential grid (more sectors).

b) An odd number of sectors.

c) A nonequiangular sector distribution.

d) A finer axial grid in the blade free volumes.

---

*It should be noted that although the static pressure is plotted using linear interpolation between the midpoints of each sector, the predicted model distribution is represented by the inset schematic.

Figure 10. Volume Exit Static-Pressure Distributions.

ORIGINAL PAGE IS
OF POOR QUALITY

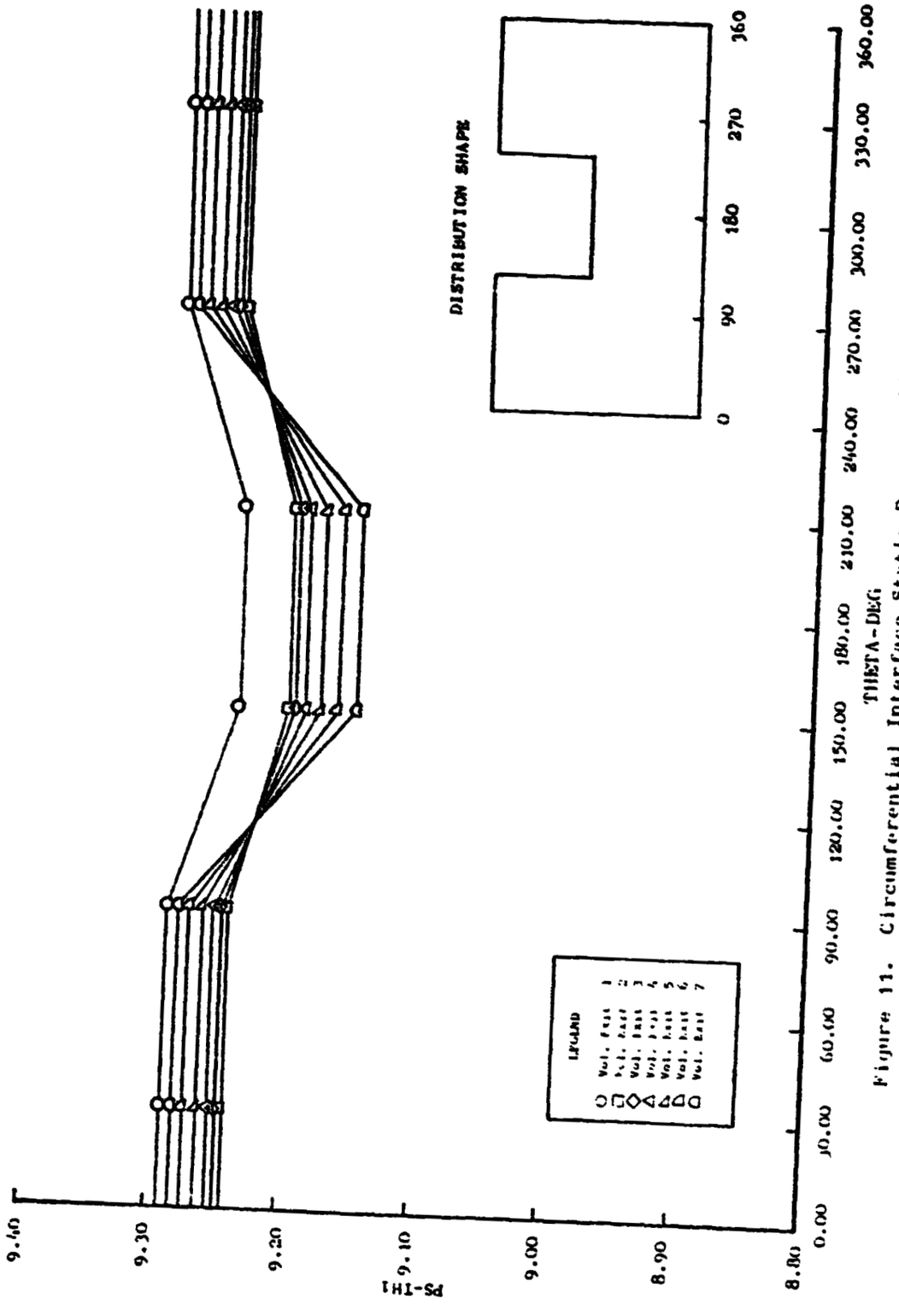

Figure 11. Circumferential Interface Static-Pressure Distributions.

In order to obtain an understanding of these items, model configurations of twelve equal 30° sectors, eleven equal 32.727° sectors, and eleven sectors (one 60°, ten 30°) corresponding to above items a, b, and c, respectively (see Figure 12) were used for these studies.

The volume axial-exit circumferential static-pressure distributions are plotted for the volume 1 exit in Figure 13 with the six 60° sector distribution superposed. The volume axial exit circumferential pressure distributions are plotted in a similar manner for the volume 7 exit in Figure 14. The important features of these figures can be summarized as follows:

1. A finer angular extent grid does not remove the side lobes or even reduce their magnitude.

2. The occurrence of the side lobes is not related to whether the compressor face flow is divided into an even or odd number of sectors.

3. The occurrence of the side lobes is not related to whether the sectors are of equiangular extent.

An attempt was made to run with some 15° sectors adjacent to the distorted region in belief that even a finer grid in the region of high gradients might give better circumferential distributions. Unfortunately, this case would not run although no significant expenditure of time was made to circumvent the incurred problems.

The effect of a finer axial grid was examined by increasing the number of blade free axial volumes upstream of the compressor IGV from seven to twelve in the six 60° sector model (see Figures 13 and 14). Again no significant improvement was noted, since the volume 1 exit static-pressure side lobes have magnitudes approximately equal to the distorted sector static-pressure, and at the exit of the last blade free volume, the results are essentially equivalent to the six 60° sector model.

Upon considering the 100% corrected speed line, it was decided to investigate only the "worst" case configuration of a 60°, 1/rev circumferential total-pressure distortion. This case required considerable effort to settle out as the distortion level was 10.6% (MAX-MIN)/AVG) and care had to be exercised to avoid computational problems due to the initially large start-up gradients. Figure 15 illustrates the resultant operating points of the sectors and the comparison with the parallel-compressor solution. Documentation of the axial flow, flow angle, and tangential-flow distributions in the blade-free volumes is provided by Figures 16 through 18 respectively.

Since the 80% corrected speed throttling simulation showed little change when compared to the parallel-compressor model predicted stability limit and since the 100% corrected-speed sector operating points are close to the parallel-compressor operating points, it was decided that a throttling simulation at 100% corrected speed was not justified.

Figure 12. Section Centerline Loads

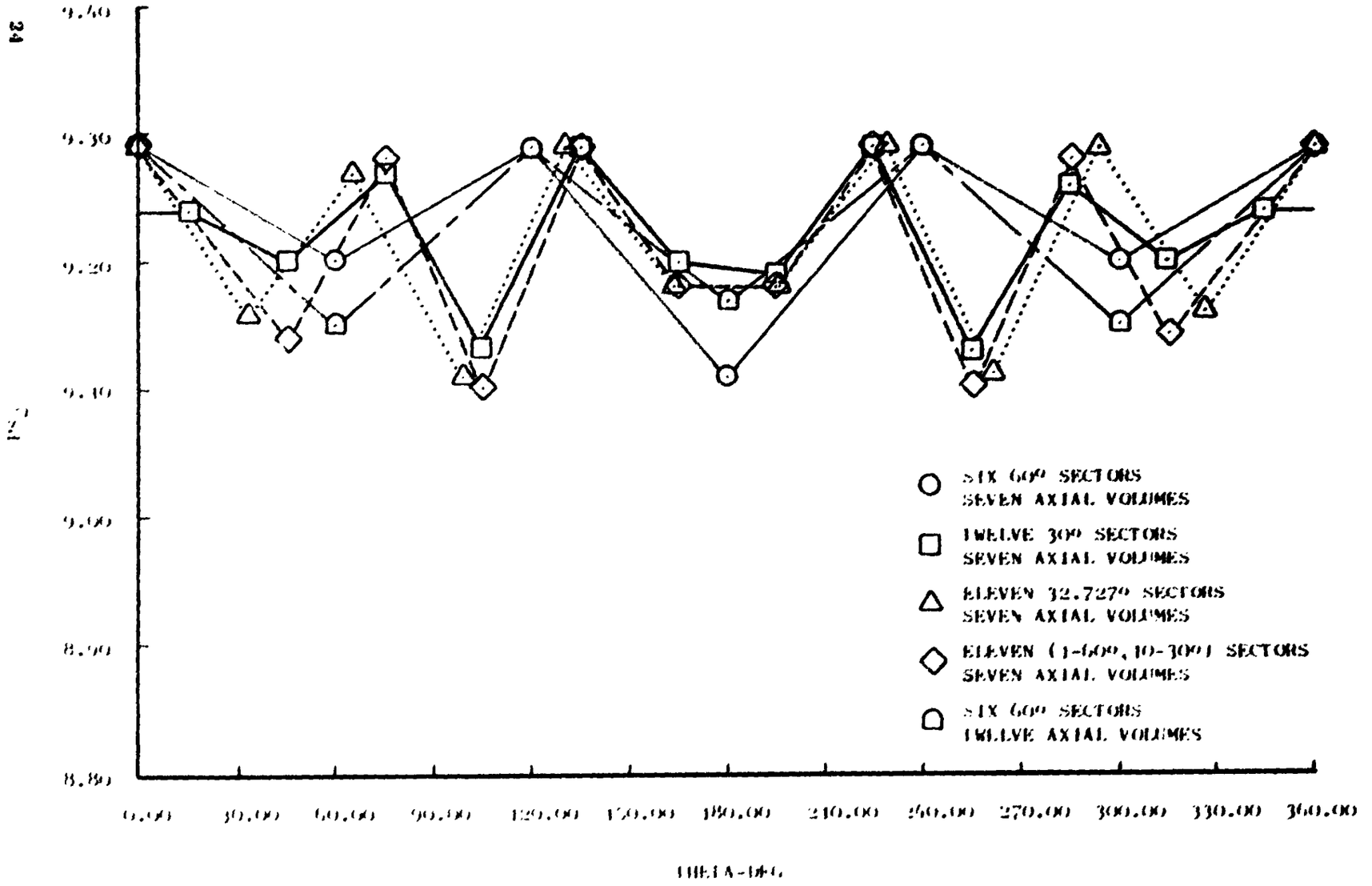

Figure 13. Volume 1 Exit Circumferential Static-Pressure Distributions.

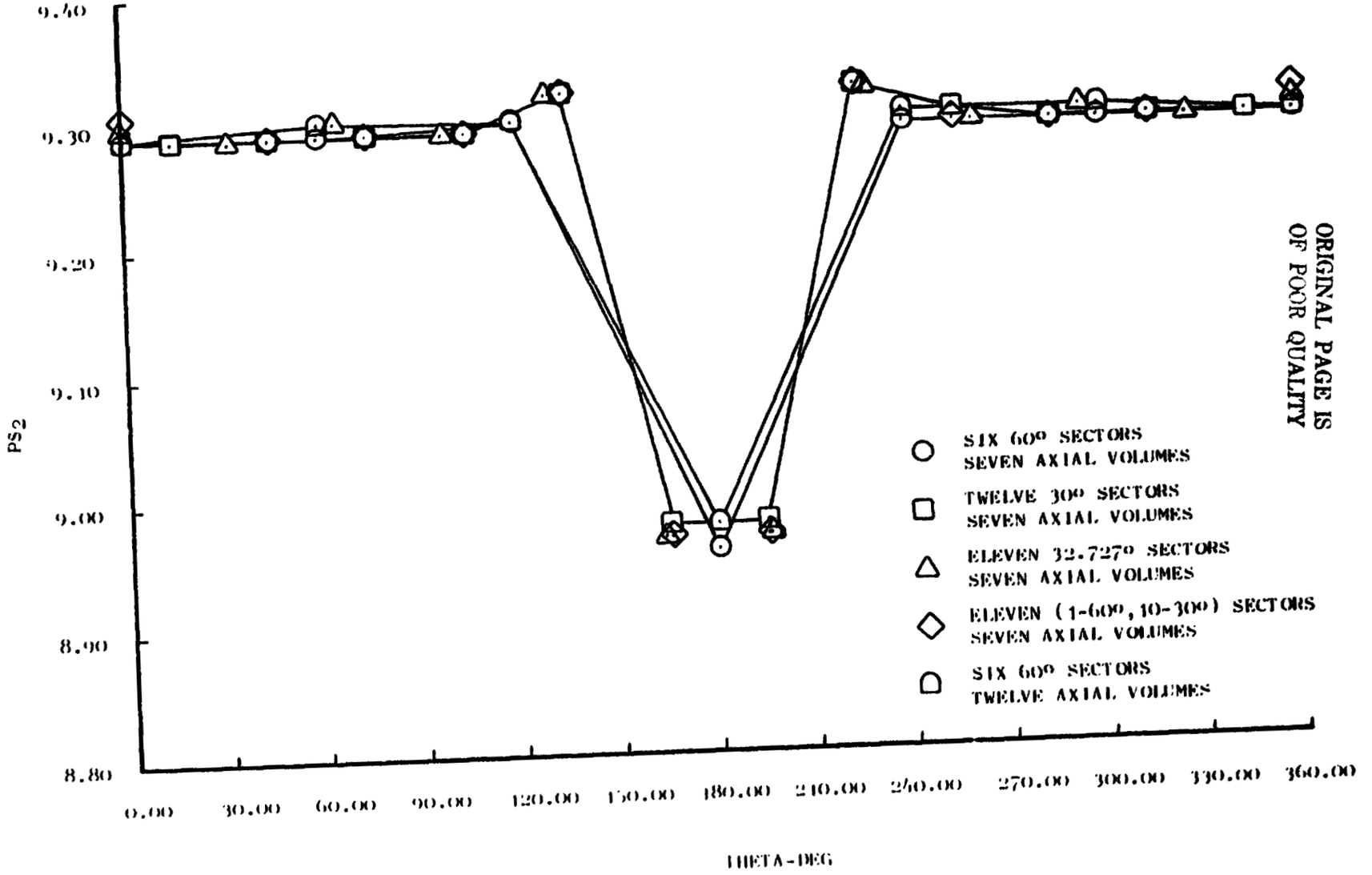

Figure 14. Compressor-Face Volume Exit Circumferential Static-Pressure Distributions.

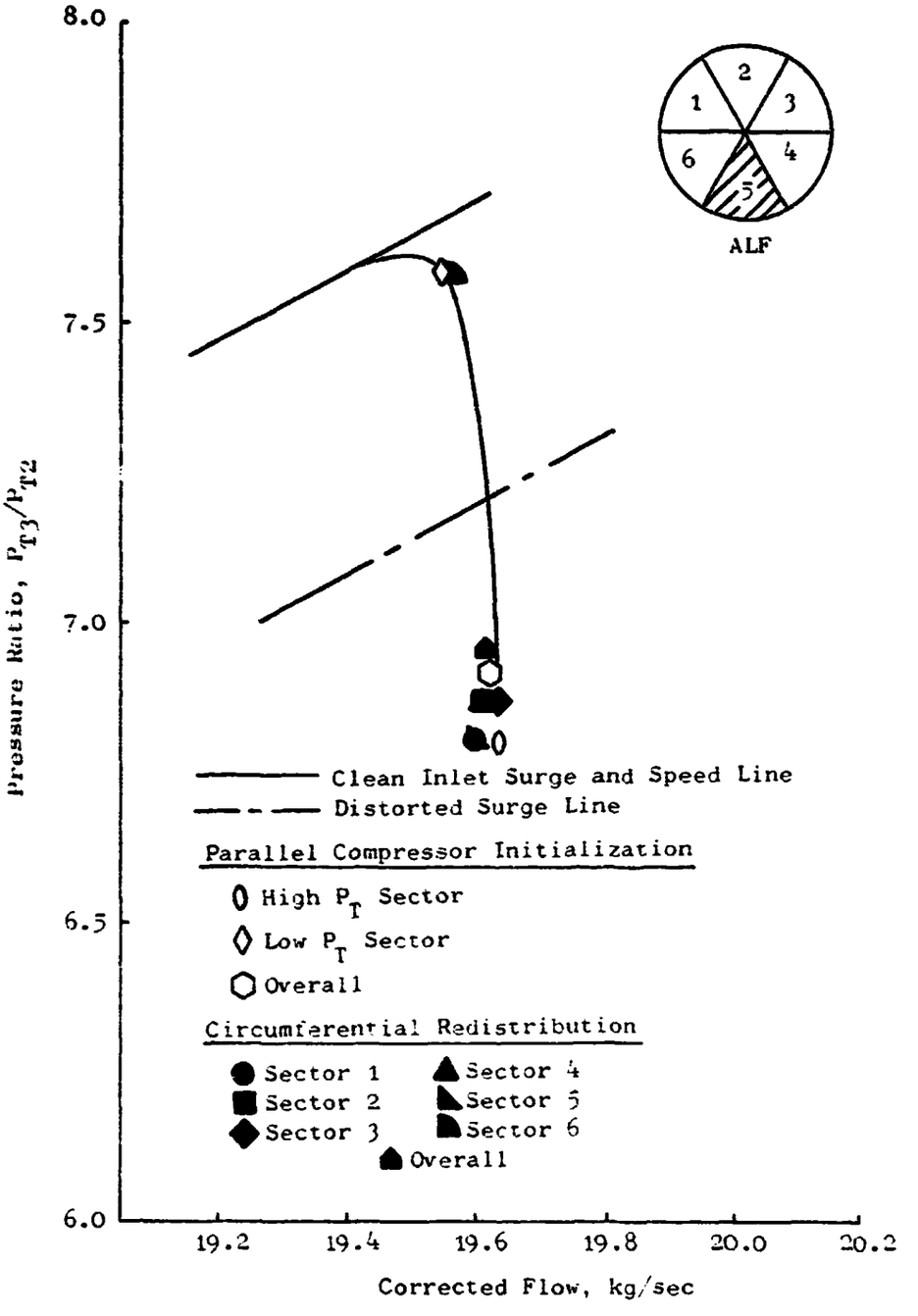

Figure 15. Circumferential Redistribution Analysis of "Moss" J85-13 Engine With 60°, 1/rev Total-Pressure Distortion. 100% $N/\sqrt{\theta}$ - Sector Performance.

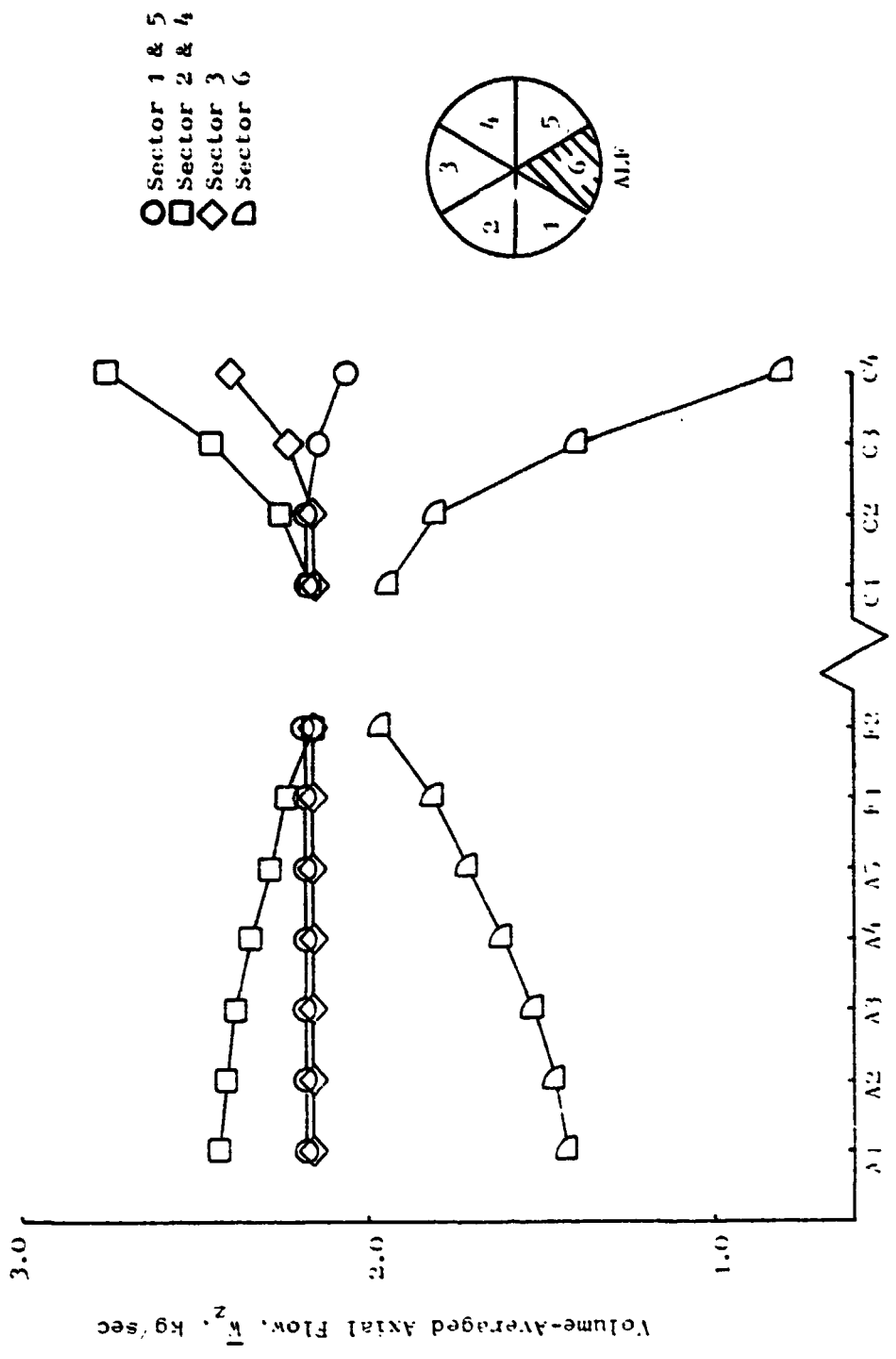

Figure 16. Circumferential Redistribution Analysis of "Moss" J85-13 Engine With 60°, 1/rev Total-Pressure Distortion, 100% $N_c/\sqrt{\theta}$ – Axial Flow Distribution.

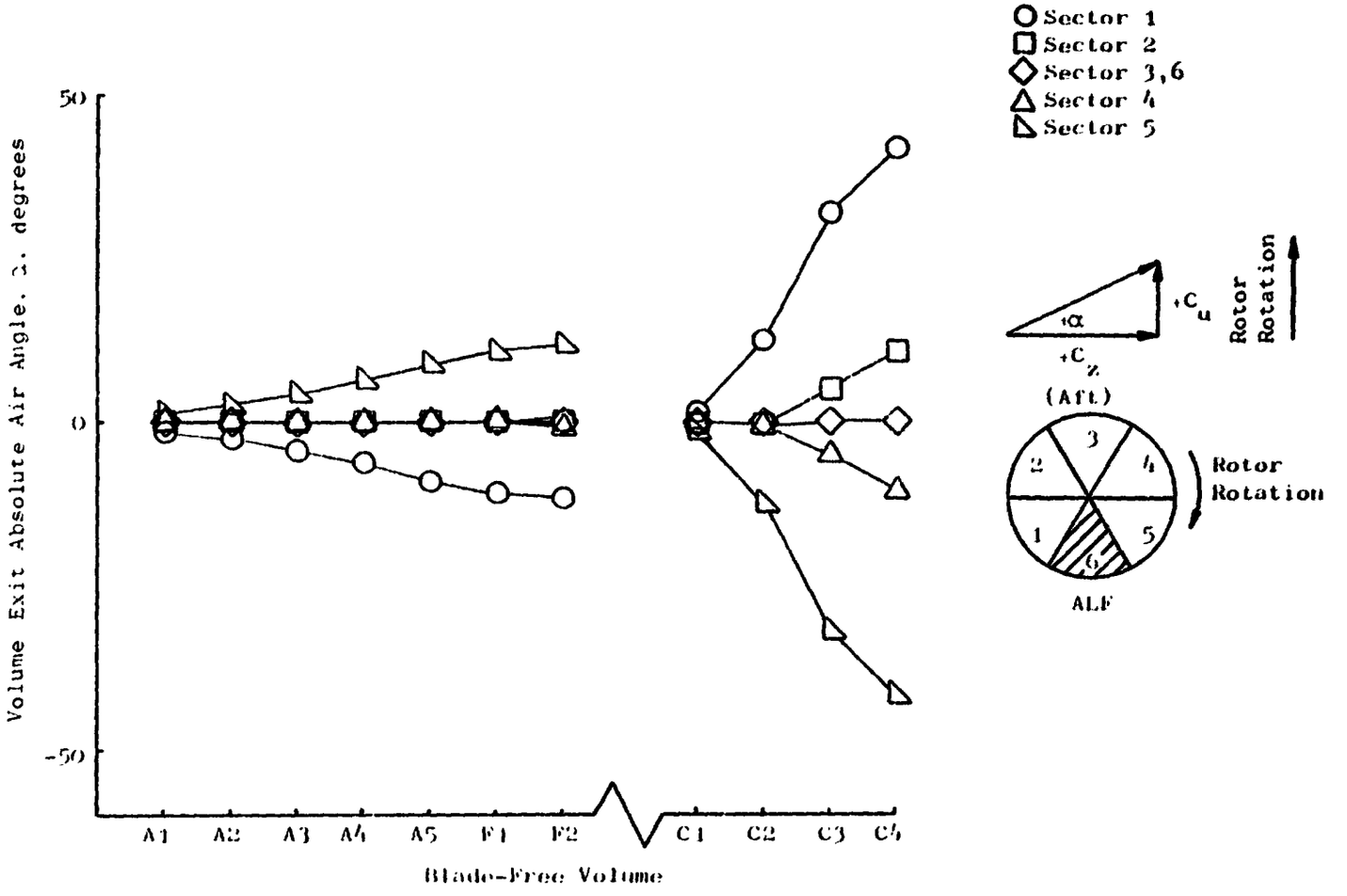

Figure 17. Circumferential Redistribution Analysis of "Moss" J65-13 Engine With 60°, 1/rev Total-Pressure Distortion, 100% $N/\sqrt{\theta}$ - Flow Angle Distribution.

ORIGINAL PAGE IS
OF POOR QUALITY

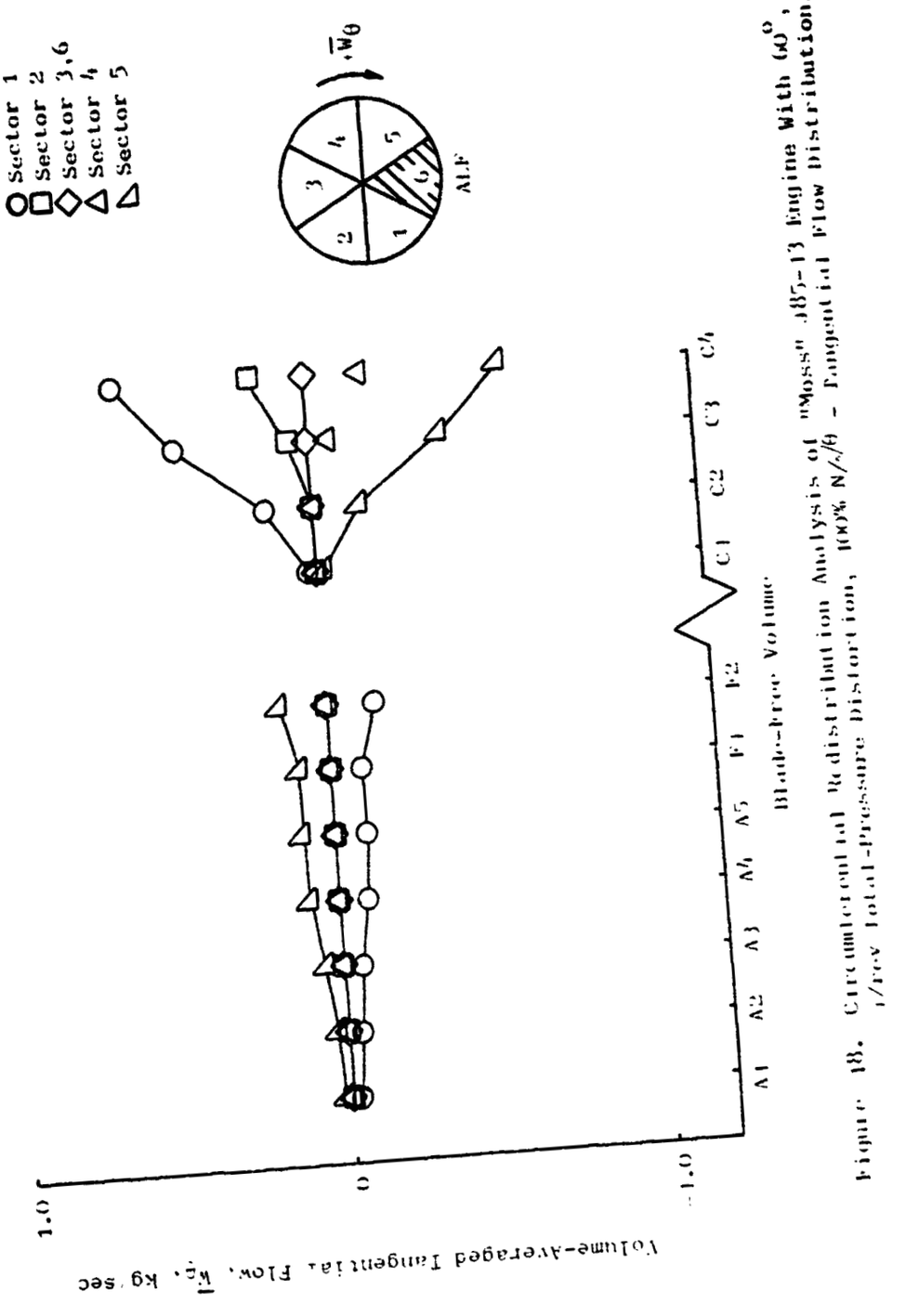

Figure 18. Circumferential Redistribution Analysis of "Moss" 185-13 Engine With 60°, 1/rev Total-Pressure Distortion, 100% N_A/θ - Tangential Flow Distribution.

3.4 REDISTRIBUTION ANALYSES SUMMARY

The results of the analyses discussed in the previous section indicate that it is possible to calculate some of the characteristics of flow redistribution in the blade-free volumes of a compression component using a coarse grid. That is, use of sectors of large angular extent can be used to obtain the gross characteristics of the flow field which it is hoped are suitable for conducting stability analyses. However, there are some aspects of the calculations which cannot be improved by either increasing the fineness of the circumferential or axial grids. It is strongly suspected that the presence of the static-pressure side lobes is a result of the algorithm used to define sector interface values in the circumferential direction. The flowfield at the entrance to the IGV's intuitively appears to be correct and thus, holds promise for providing better compressor entrance conditions for use in stability calculations. If one's main interest were the details of the flowfield, then it probably would be necessary to resort to a differential formulation.

While the prediction of the major characteristics of the flowfield is of interest in itself, it has not improved the ability to predict the loss in surge pressure ratio due to distortion, expecially at low speeds for the J85-13 compressor. Although there are a number of possible explanations for this apparent deficiency, it is suspected that two of the more significant explanations are: 1) the presence of the IGV and how it is modeled; and 2) the dynamic response of the rotors.

For this model of the J85-13 engine, the inlet guide vanes are modeled as a lossless blade-row having constant deviation angle along any particular speed line. This constraint forces the exit air angle of the IGV to remain a constant, regardless of the incidence angle to which it is subjected. For example, Figure 4 indicates a 23° range in air angle at the IGV inlet and yet the exit air angle and loss are the same for all sectors. However, the removal of this constraint would require test data which generally is not available. It is anticipated that a simulation of a fan with no IGV would exhibit considerably more response to the effects of redistribution since the rotor 1 loss coefficients and deviation angles will vary from sector to sector as the incidence angle varies from sector to sector.

An additional item of concern is that parallel-compressor type solutions doe not address the problem of the dynamic response of the rotors as they travel through the distortion pattern. A preliminary investigation into the dynamic blade row response was performed in an attempt to gain some insight into the magnitude of this effect and is discussed in the following section.

3.5 DYNAMIC BLADE-ROW RESPONSE

One of the standard assumptions used in parallel-compressor type analyses is that the compression component of each sector responds independently and as if each were experiencing clean inlet flow. This implies that each sector responds instantaneously to circumferential variations in incidence

angle. During the simulation of planar pressure waves in a two-stage fan (Reference 8), it was found that above certain frequencies the blade response could not be adequately represented with an instantaneous response, but rather provision for the dynamic response had to be made in order to obtain a better representation of the blade row performance. It was the purpose of the following analysis to formulate a dynamic response function for blades entering and leaving circumferentially distorted regions and at the same time retain the economical computational advantages of a parallel-compressor type solution. The method proposed in this report for representing the aerodynamic blade response to circumferential distortion builds upon the blade response function developed for blade rows subjected to planar waves in Reference 8 and the work of Kimzey (Reference 9).

The response of a blade row to changes of instantatous incidence angle can be expressed as:

$$\tau \frac{\partial(i_e - i_o)}{\partial t} + (i_e - i_o) = i_i - i_o \qquad (7)$$

where τ is the blade row time constant, i_e is the effective incidence angle, i_i is the instantaneous incidence angle, and i_o is a reference incidence angle. The dependent variable, effective incidence angle, is defined as the incidence angle which is equivalent to the dynamic response of the blade as it passes through the distortion. This implies that the blade-row characteristics are functions of the effective incidence angle rather than the instantaneous incidence angle. This formulation permits working with only one differential equation and can account for the blade response to a step change in the actual incidence angle.

With reference to Figure 19a and a parallel compressor model, the quantity i_i is the step change in actual incidence angle and i_o is the previous sector effective incidence angle as the blade leaves the sector. Solving Equation (7) for the homogeneous and particular solutions for the step change in incidence angle of Figure 19a yields

$$i_e = i_{i_2} + (i_{i_1} - i_{i_2})\, e^{-t/\tau} \qquad (8)$$

The effective incidence angle response for a large angular extent distortion where the effective incidence angle rises essentially to the instantaneous value of incidence angle is shown in Figure 19a. The effective incidence angle response for a small angular extent distortion, where the effective incidence angle will not rise to the instantaneous incidence angle before the blade leaves the distorted region is shown in Figure 19b. Notice that in this case, the starting point (reference value) for the effective incidence angle calculation in the undistorted region is the last value of the effective incidence angle in the distorted region.

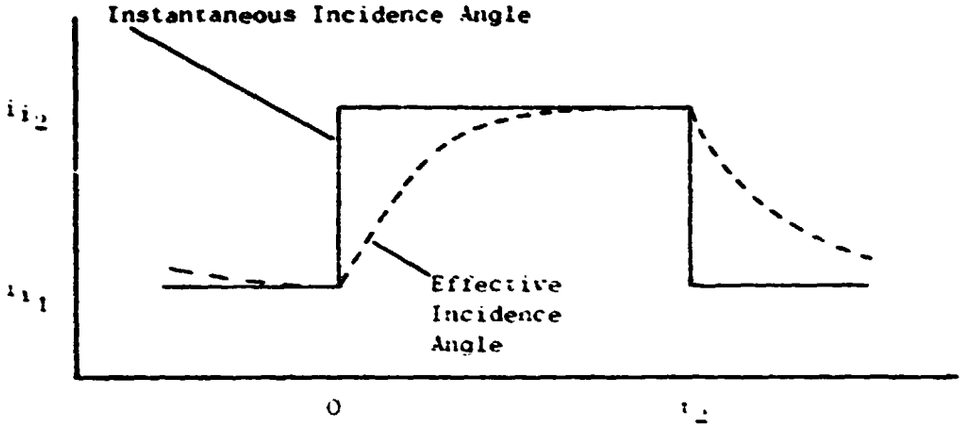

a) Large Extent Distortion

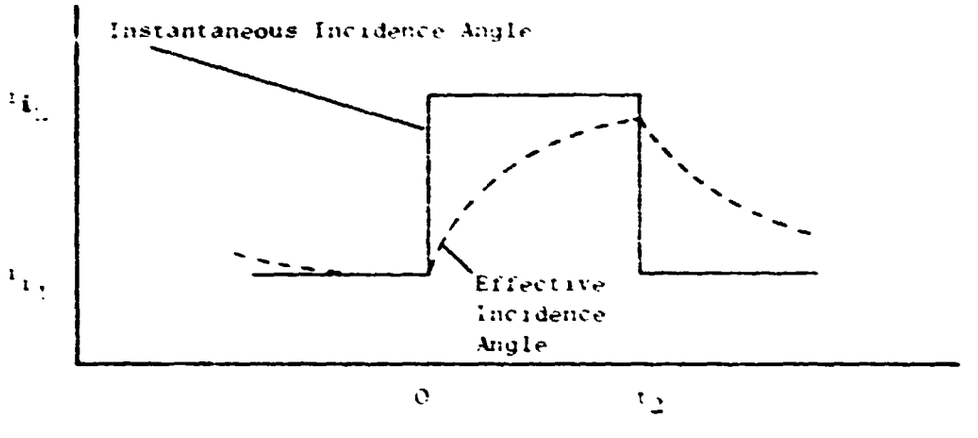

b) Small Extent Distortion

Figure 19. Dynamic Rotor Response Schematic.

Before the effective incidence angle can be used in a parallel compressor model, it should be noted that the flow in each sector is an average flow for that sector. Hence, the corresponding effective incidence angle to be used in the parallel compressor calculations is an average (mean) effective incidence angle for each sector. Integration of Equation 8 over the interval (0 to t_2) that the blade is within the sector gives

$$\bar{i}_e = \frac{1}{\Delta t}\int_0^{t_2} i_e\, dt = \frac{1}{t_2}\left[i_{i_2}\, t_2 + (i_{i_2} - i_{i_1})\, \tau\, (e^{-t_2/\tau} - 1) \right] \qquad (9)$$

as an expression for the mean effective incidence angle. Since only rotor blade rows move into and out of disturbances in a steady distorted flow, Equation 9 is applied only to rotors and the mean effective incidence angle rather than the instantaneous incidence angle is used to determine the rotor loss coefficients and deviation angles. Therefore, it remained to determine the time constant of Equation 9 that best represented the test results. This was accomplished by evaluating different values of τ until an improved data match between the model results and the test data was obtained in terms of ΔPRS. Since it had been well established in Reference 1 that the dynamic parallel-compressor stability limit was reached when the distorted-sector speed-line slope went to zero, it was felt that there was no need for dynamic simulations during this preliminary investigation. Therefore, this effort was performed through the use of the steady-state parallel-compressor model, modified accordingly for the calculation of the effective incidence angle.

The time constant in keeping with Reference 8 and the work of others (Reference 9) was defined to be proportional to the chord of the rotor divided by the inlet relative velocity; or in other words, some multiple of the time it takes a particle to travel through the blade row.

$$\tau = \frac{A\, c}{W'_1} \qquad (10)$$

The same time constant was used for each blade row rather than varying it as a function of solidity as was done in Reference 8.

An attempt was made to determine an optimum value of the proportionality constant A at each speed (80% and 100% $N/\sqrt{\theta}$ for each distortion (180° and 60° 1/rev) by choosing the integer value from Figure 20 which gave the least error between the predicted and measured values of ΔPRS. The 180°, 1/rev simulations were performed using a two 180° sector model while the 60°, 1/rev simulations were performed using a two sector model with a 300° clean-inlet-flow sector and a 60° distorted-inlet-flow sector. The speed line and predicted surge point for each distortion pattern and speed with the selected value of A are given in Figures 21 through 23. Unfortunately, it was not possible to obtain a solution for values of A greater than 2 for the low flow sector for the 60° extent distortion at 80% corrected speed. The lack of results with

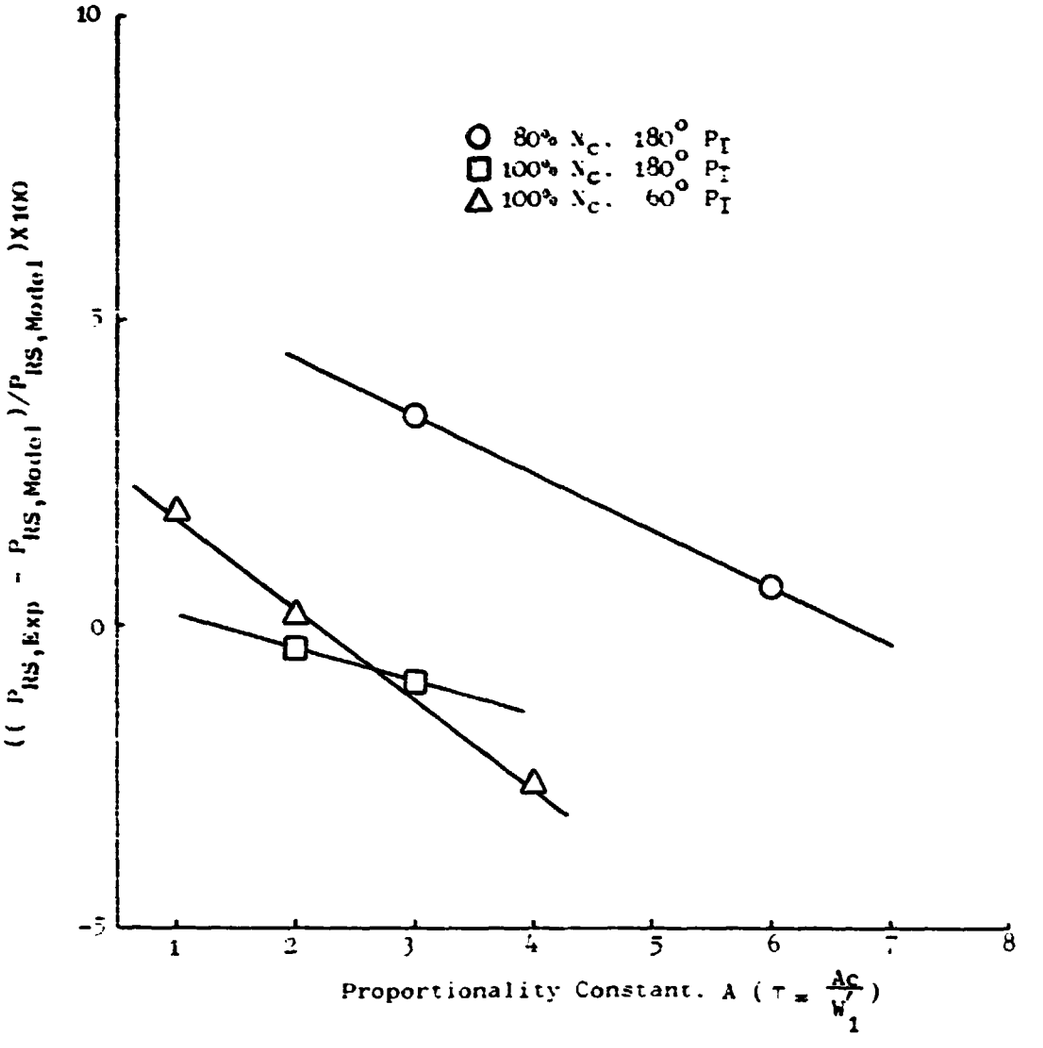

Figure 20. Time Constant Impact on the Prediction of the Inlet Total-Pressure Distortion Stability Point.

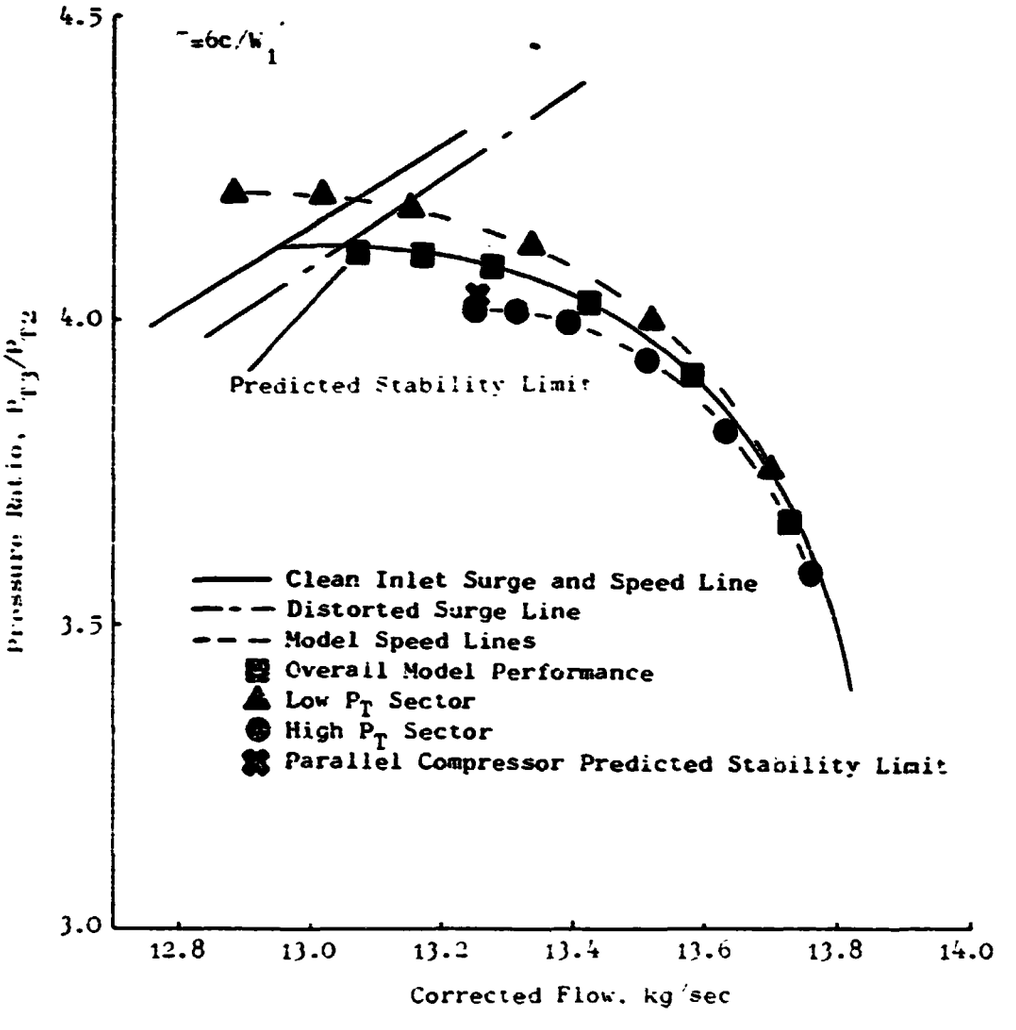

Figure 21. Dynamic Rotor Response Analysis of "Moss" J85-13 Engine With 180°, 1 rev Total-Pressure Distortion, 80% N/$\sqrt{\theta}$.

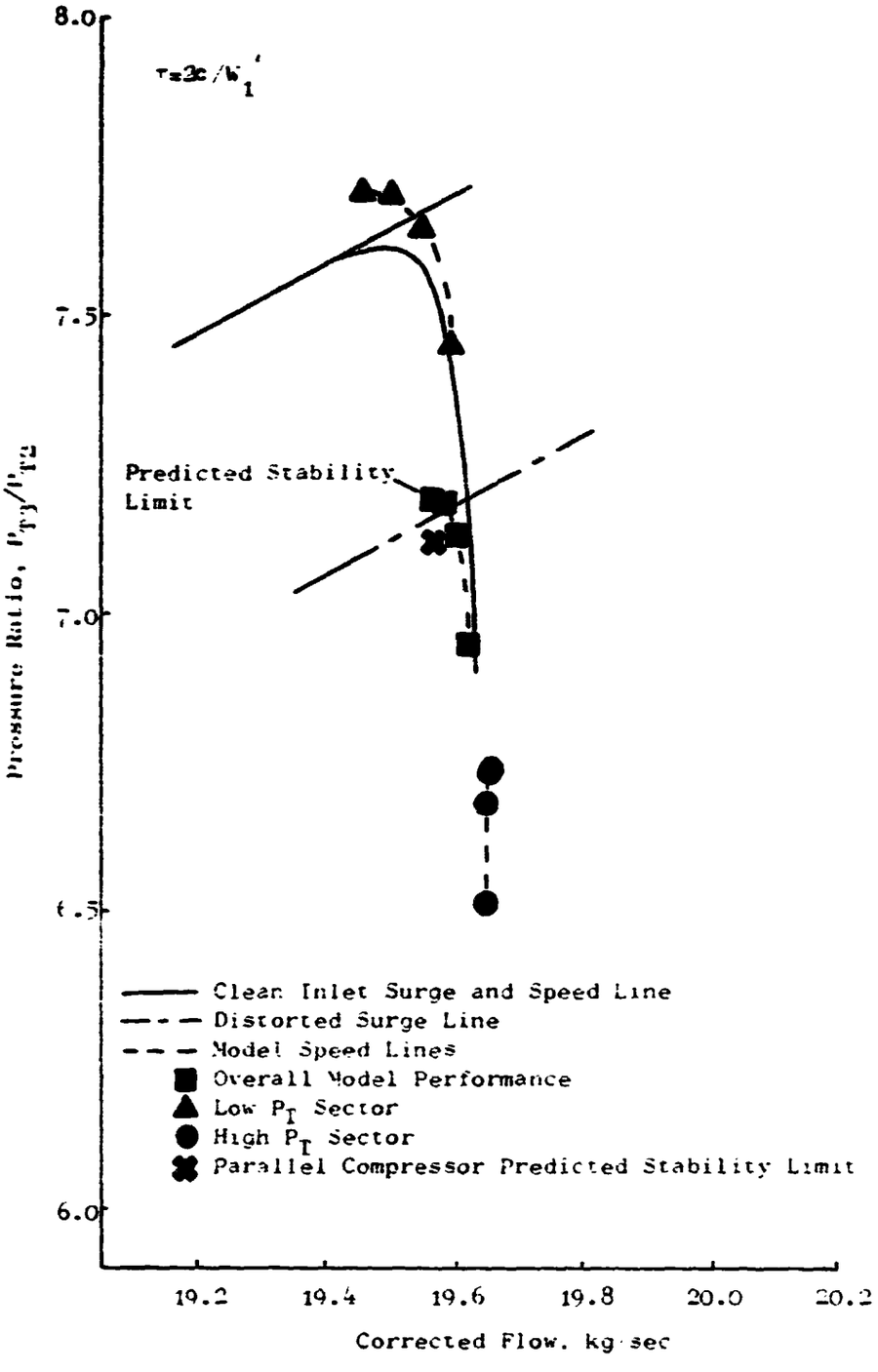

Figure 22. Dynamic Rotor Response Analysis of "Moss" J85-13 Engine With 180°, 1/rev Total-Pressure Distortion, 100% $N/\sqrt{\theta}$.

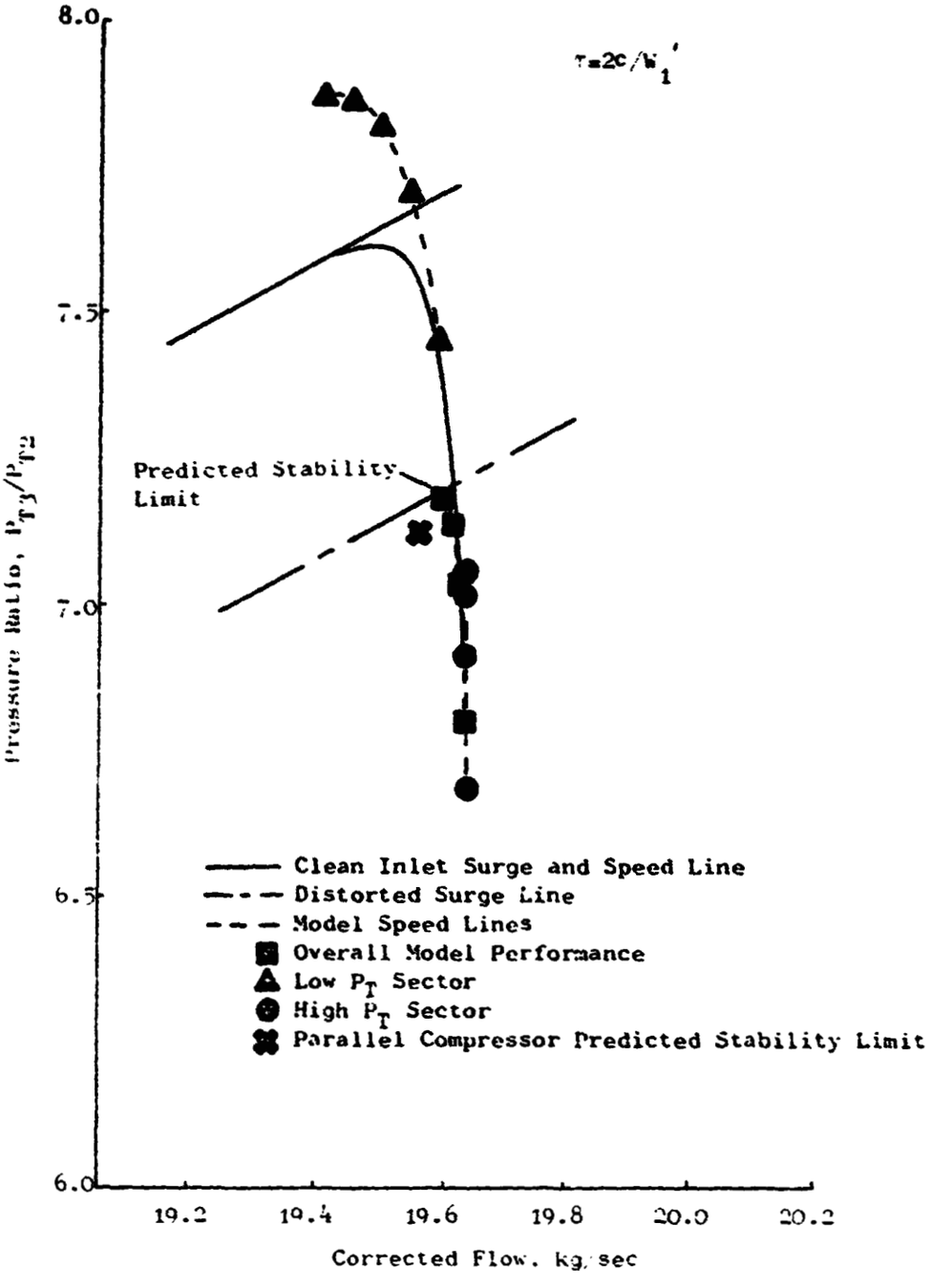

Figure 23. Dynamic Rotor Response Analysis of "Moss" J85-13 Engine With 60°, 1/rev Total-Pressure Distortion, 100% $N/\sqrt{\theta}$.

the 60°, 1/rev total-pressure distortion results at 80% corrected speed represent more of a limitation of the blade row characteristics than the determination of an optimum proportionality constant. Any further increase in the constant A to a value greater than 2 pushed the performance of the distorted sector to a level where the uniform static-pressure boundary condition could not be satisfied. This is a result of severe mismatching between the clean inlet characteristics of the individual stages.

The time constants implied by the above obtained proportionality constants are one-fifth to one-half the time a blade resides in a 180° distorted-flow sector, thus indicating that the effective incidence angle has very nearly reached a value equal to the instantaneous incidence angle by the time it has completely traversed the distorted-flow region. An inspection of the proportionality constant used in the planar wave studies of Reference 8 shows that the constant obtained in this study is an order of magnitude greater than the Reference 8 proportionality constant. It was recognized that the planar wave proportionality constant, which was based on an incompressible, inviscid analysis, was too small to permit proper representation of the blade row response to planar waves. Further, the time constant developed for the circumferential distortion analyses implicitly takes into account the phase lag between the blade passages within a blade row operating in a distorted flow region and the flow field edge effects associated with the low pressure region of the distortion pattern.

3.6 DYNAMIC BLADE-ROW RESPONSE SUMMARY

Comparison of the experimental, parallel-compressor, and parallel-compressor with dynamic blade-row response surge points presented in Figures 21 through 23 show that there is considerable gain to be realized when the blade-row dynamic response is taken into account. Even with the preliminary formulation given in this report, significant improvements over the parallel-compressor analyses can be made. It appears, however, that the same value of proportionality constant (Equation 9) is not applicable for all speeds. This would tend to indicate that the proportionality constant is dependent on some combination of the flow conditions that change as a function of speed.

4.0 VARIABLE STATOR LOSS

During the dynamic blade-row stability analyses performed in the previous section and in Reference 1, the losses for an entire stage were assigned to the rotor. The stator had no losses assigned to it and possessed a constant deviation angle. This distribution of losses within a stage was not a constraint of the model, but rather was dictated by the test data which did not lend itself to distributing the losses between the rotor and the stator. It was the purpose of this study to evaluate the impact of variable stator losses on the behavior of the dynamic model. Since it was desired to avoid an extensive restacking of the compressor, each individual stage was held to the same overall total-pressure and total-temperature characteristic with or without the inclusion of stator losses. Thus, the overall stage characteristics and the stator deviation angle were held invariant, while new rotor loss coefficients and deviation angles were derived assuming a stator loss distribution based upon cascade data and correlations. Evaluation of the effect of variable stator losses was performed through a series of clean-inlet throttling simulations using the dynamic analysis computer model. The results obtained from these simulations were compared with results obtained during the Reference 1 study in which stator losses were not included.

4.1 DETERMINATION OF ROTOR AND STATOR LOSS DISTRIBUTIONS

Stator loss distributions were generated using a correlation technique based on experimental cascade test data. The correlation included the influence of parameters such as solidity, turning angle, incidence angle, inlet Mach number and diffusion factor. Once the stator loss distributions were established, the resultant rotor loss and deviation angle distributions were determined using a derivative of the steady-state program (Reference 1) with the constraint that the overall total-pressure and total-temperature stage characteristics remain unchanged. Figures 24 through 29 present the rotor loss and deviation angle distributions and the stator loss distributions developed for use in this analysis. The inclusion of stator losses required that the drag force of the stator on the fluid be calculated. This drag force was calculated in a manner analogous to that for rotors (Reference 1) with the difference that relative quantities such as total pressure were replaced with absolute quantities. The loss coefficient was defined as the loss in total pressure across the stator divided by the stator-inlet dynamic head.

4.2 CLEAN-INLET THROTTLING SIMULATIONS

The effect of including variable stator losses on the dynamic model was evaluated by performing a series of clean-inlet throttling simulations to determine if any significant differences in dynamic response or location of instability initiation occurred. Throttling simulations were performed for the "Moss" J85-13 engine at 80% and 100% corrected speeds. Figures 30 and 31

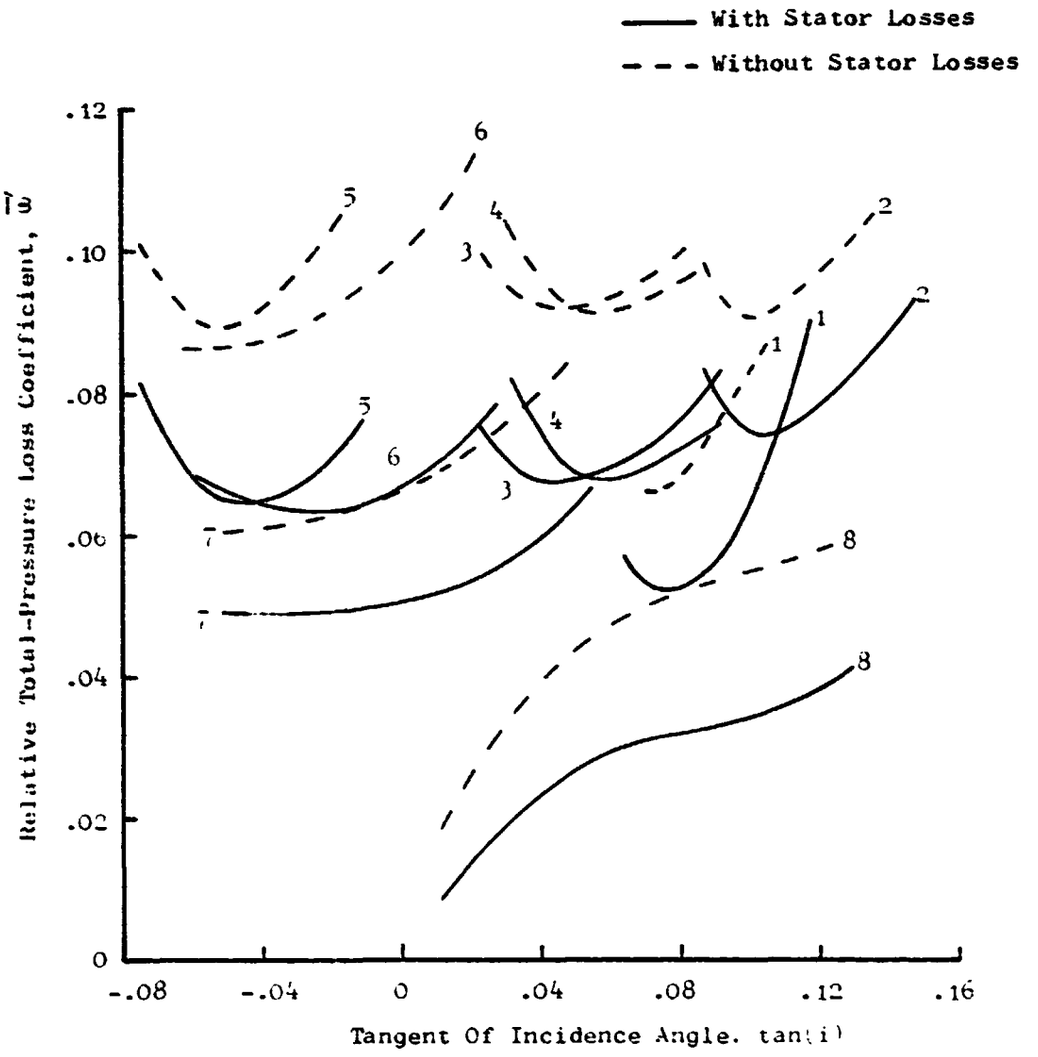

Figure 24. Rotor Relative Total-Pressure Loss Coefficients, With and Without Stator Loss; "Moss" J85-13 Engine, 80% N$_2$.

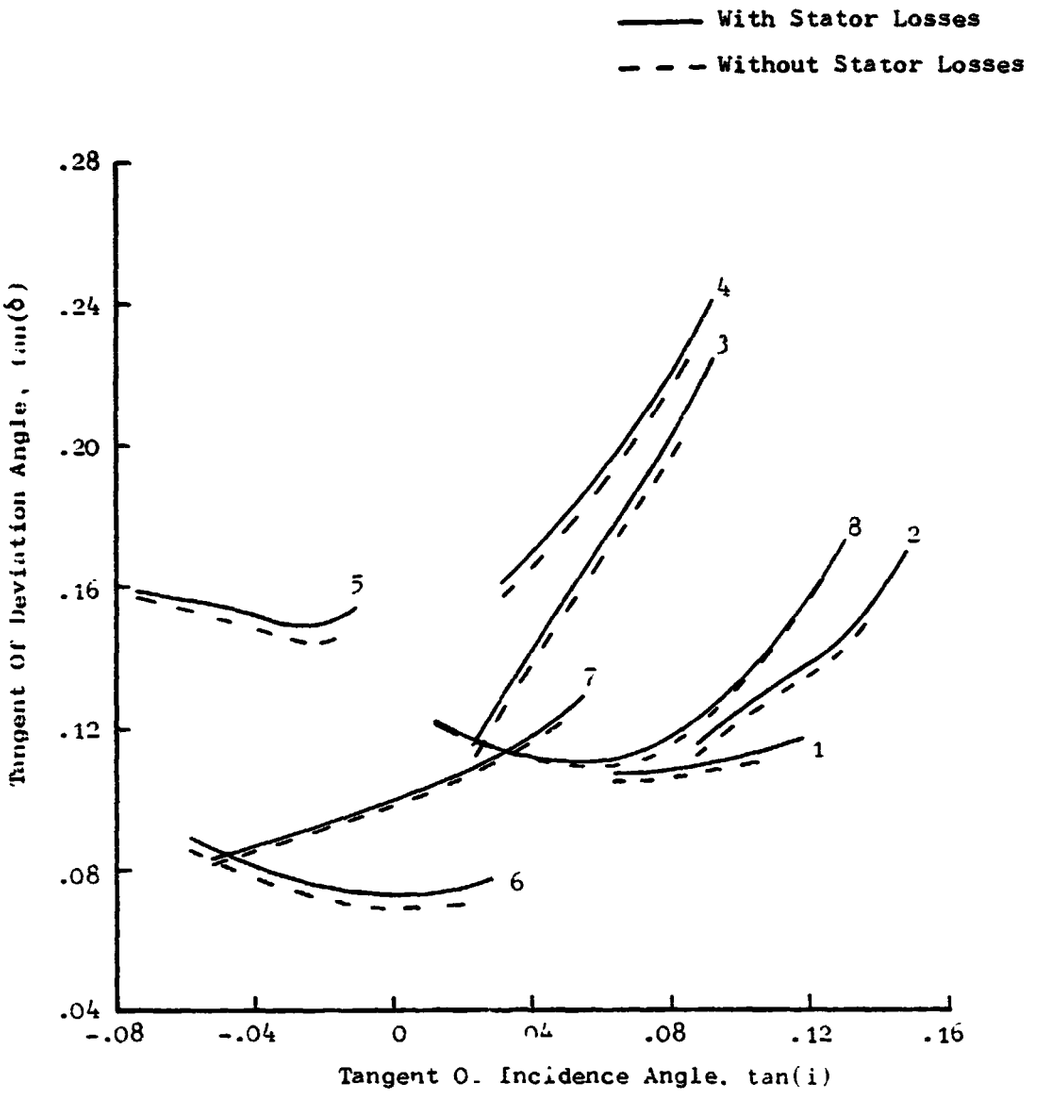

Figure 25. Rotor Tangent of Deviation Angle, With and Without Stator Loss: "Moss" J85-13 Engine, 80% N/√θ.

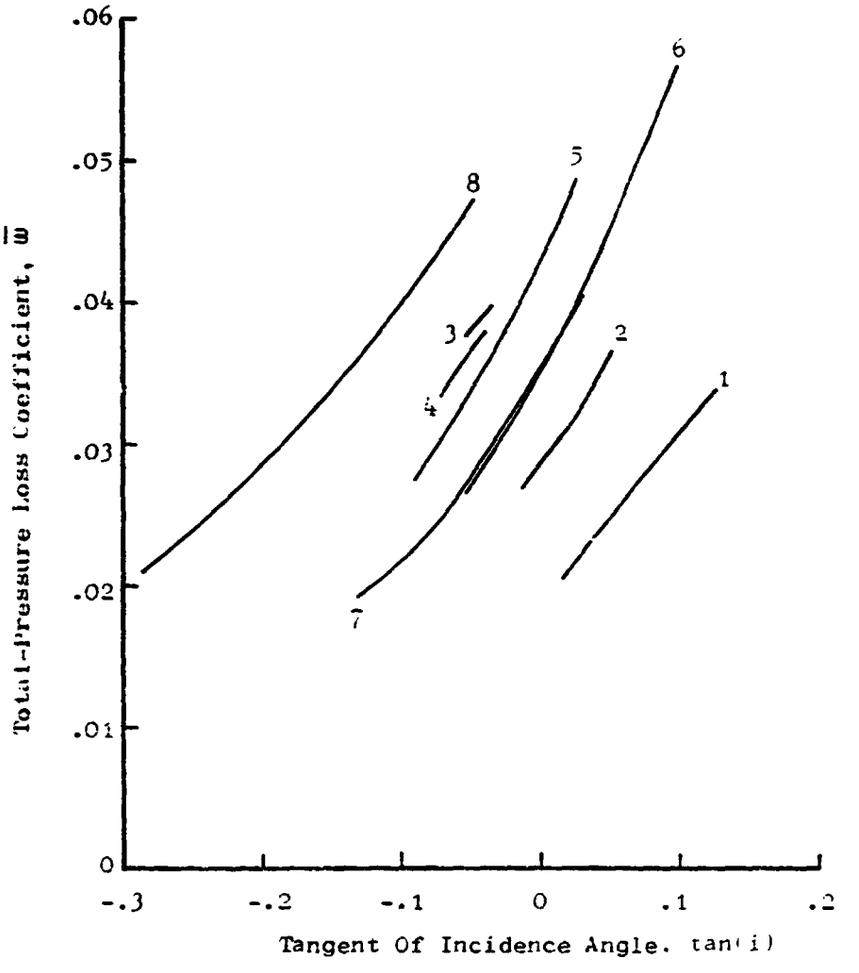

Figure 26. Stator Total-Pressure Loss Coefficients, "Moss" J85-13 Engine, 80% N$_2$.

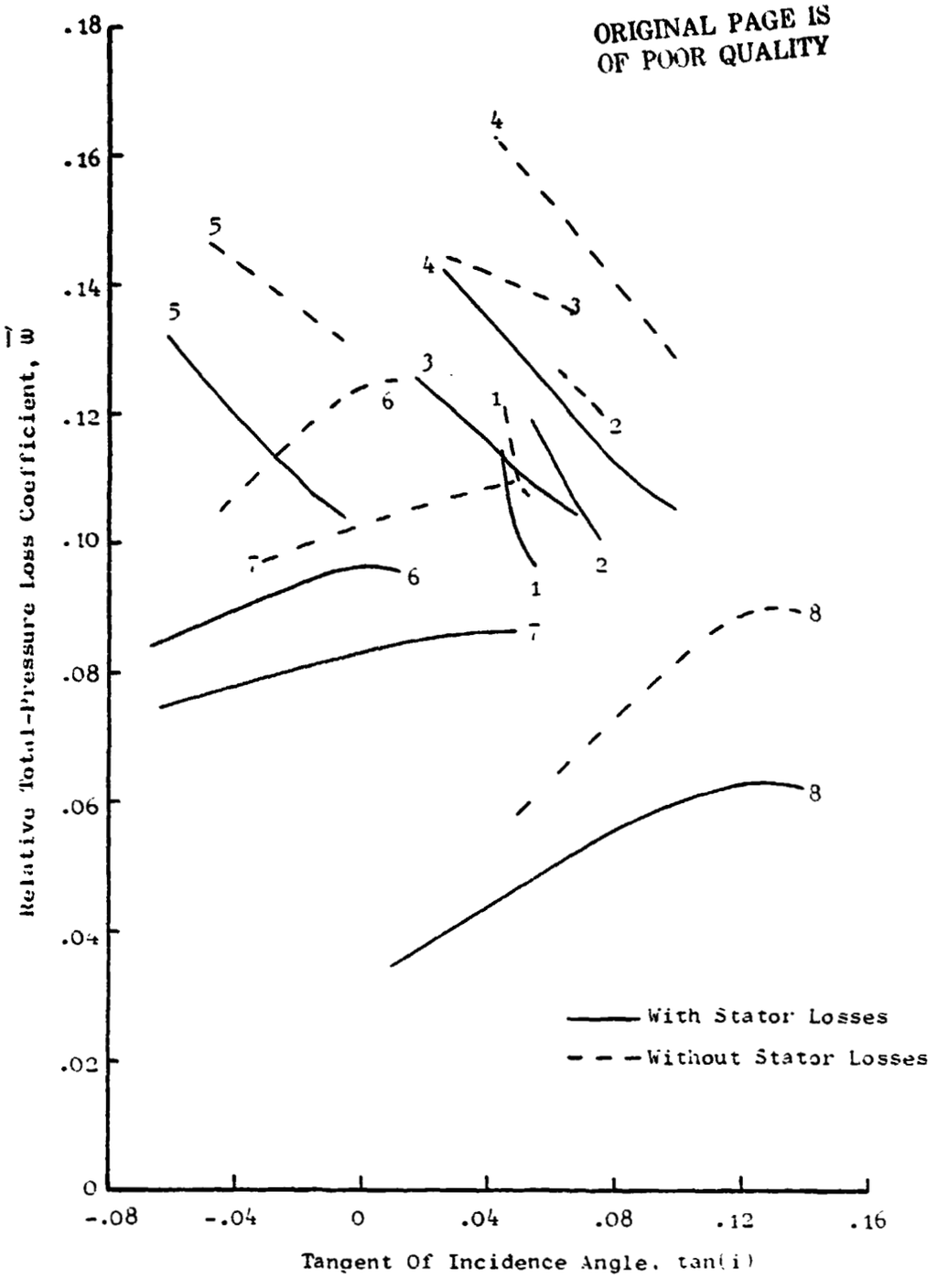

Figure 27. Rotor Relative Total-Pressure Loss Coefficients, With and Without Stator Loss; "Moss" J85-13 Engine, 100% N $\sqrt{\theta}$.

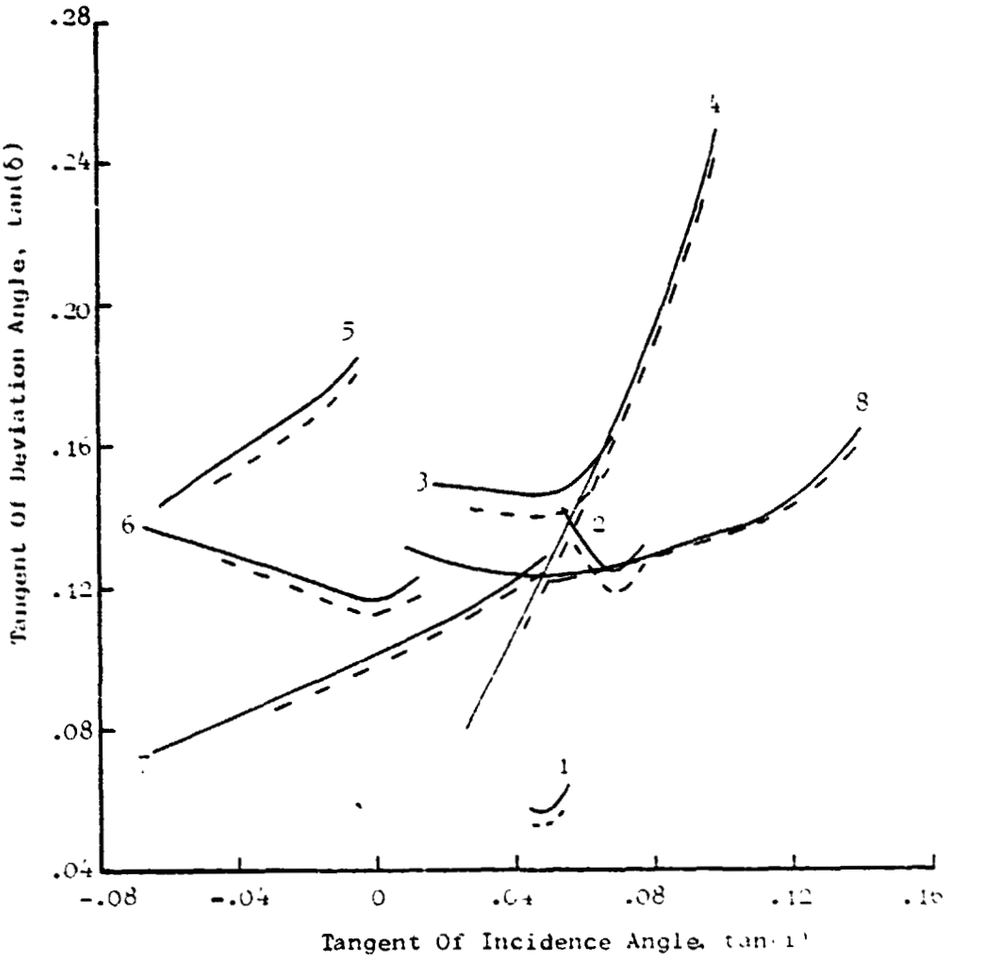

Figure 28. Rotor Tangent of Deviation Angle, With and Without Stator Loss: "Moss" J85-13 Engine, 100% N$_2$.

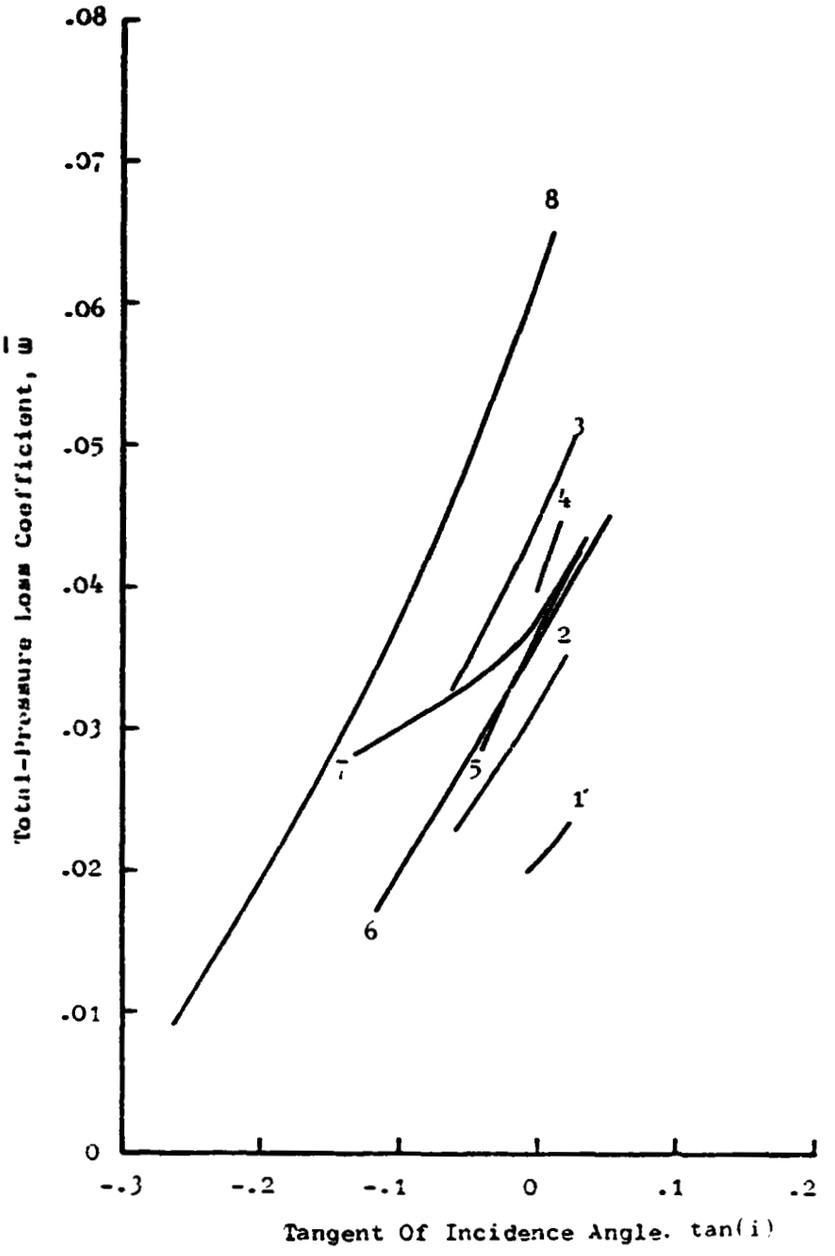

Figure 29. Stator Total-Pressure Loss Coefficients, "Moss" J85-13 Engine, 100% N$_2$.

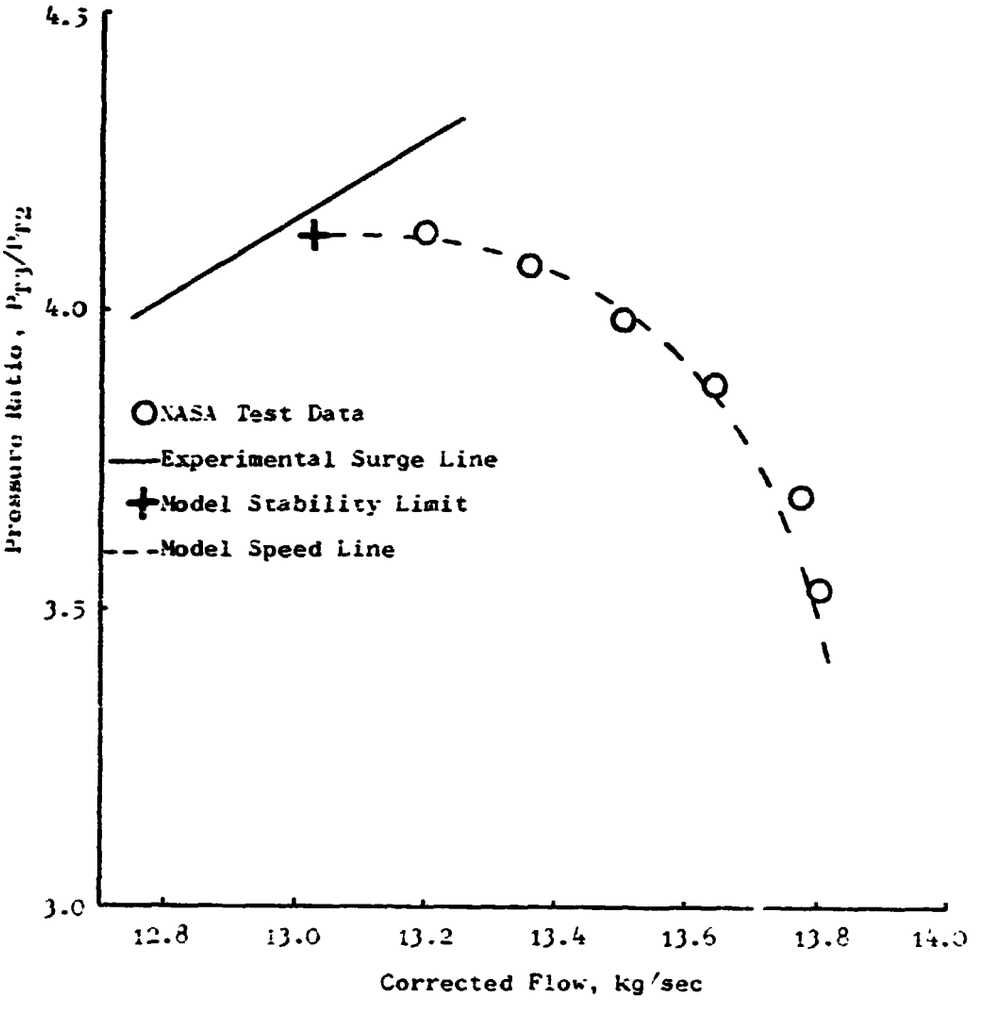

Figure 30. Clean-Inlet-Throttling Simulation, "Moss" J85-13 Engine With Stator Loss, 80% N$_2$.

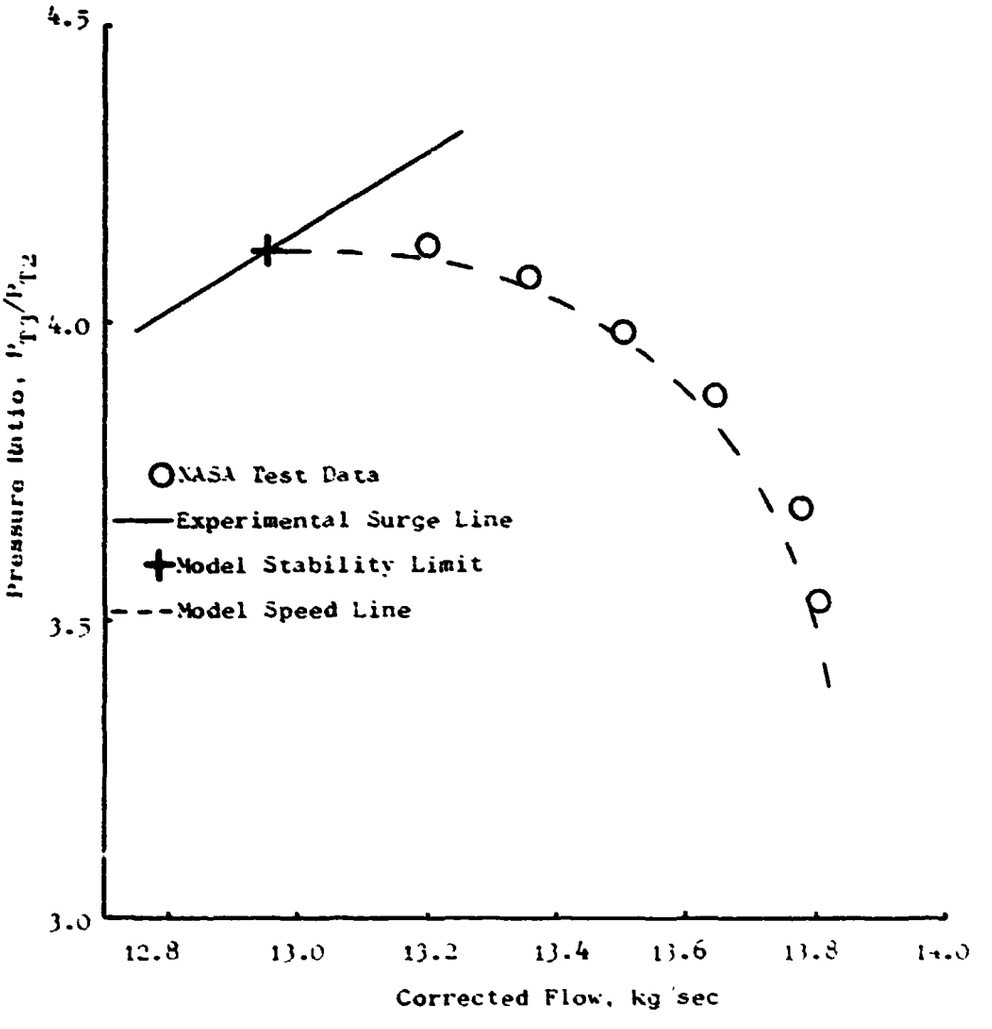

Figure 31. Clean-Inlet-Throttling Simulation, "Moss" J85-13 Engine Without Stator Loss, 80% N$_2$.

illustrate the different responses for the 80% speed line with and without stator losses, respectively. A similar comparison is shown in Figures 32 and 33 for the 100% corrected speed line. It was apparent from these throttling simulations that the indicated stability limit did not change appreciably with the inclusion of variable stator losses. However, during these simulations it was discovered that the computational time required to perform these throttling simulations was significantly reduced with the inclusion of stator loss. On the average, the inclusion of the stator losses resulted in a 23% reduction in the computational time required to throttle to the surge line.

Further, an investigation of the stability criterion, the ratio of the volume-averaged flow time derivative to the exit volume-averaged flow time derivative (amplification function), showed that when the value of this amplification function exceeded 1.5 in all volumes and the throttling process was terminated, the model would not settle into a steady-state condition. During the Reference 1 study when the stator losses were assumed to be zero, it was found that the amplification function would have to equal or exceed a value of 2.0 in all volumes before the model would not settle into a steady-state condition when the throttling process was terminated. Thus, the reduced throttling time and lower value of the amplification function for defining the surge line are evidence that the inclusion of stator losses results in increased sensitivity of the model.

Examination of the throttling simulation data below the experimental surge line indicated that the inclusion of stator losses produced no significant changes in the individual blade-row performances and no change in the locations of the stalling stage. Certain differences in flow behavior in the post-surge region were observed for the cases with and without stator losses, but it is not known whether to attribute these differences to the effect of stator losses or to the extrapolation of blade-row characteristics into the post-surge region.

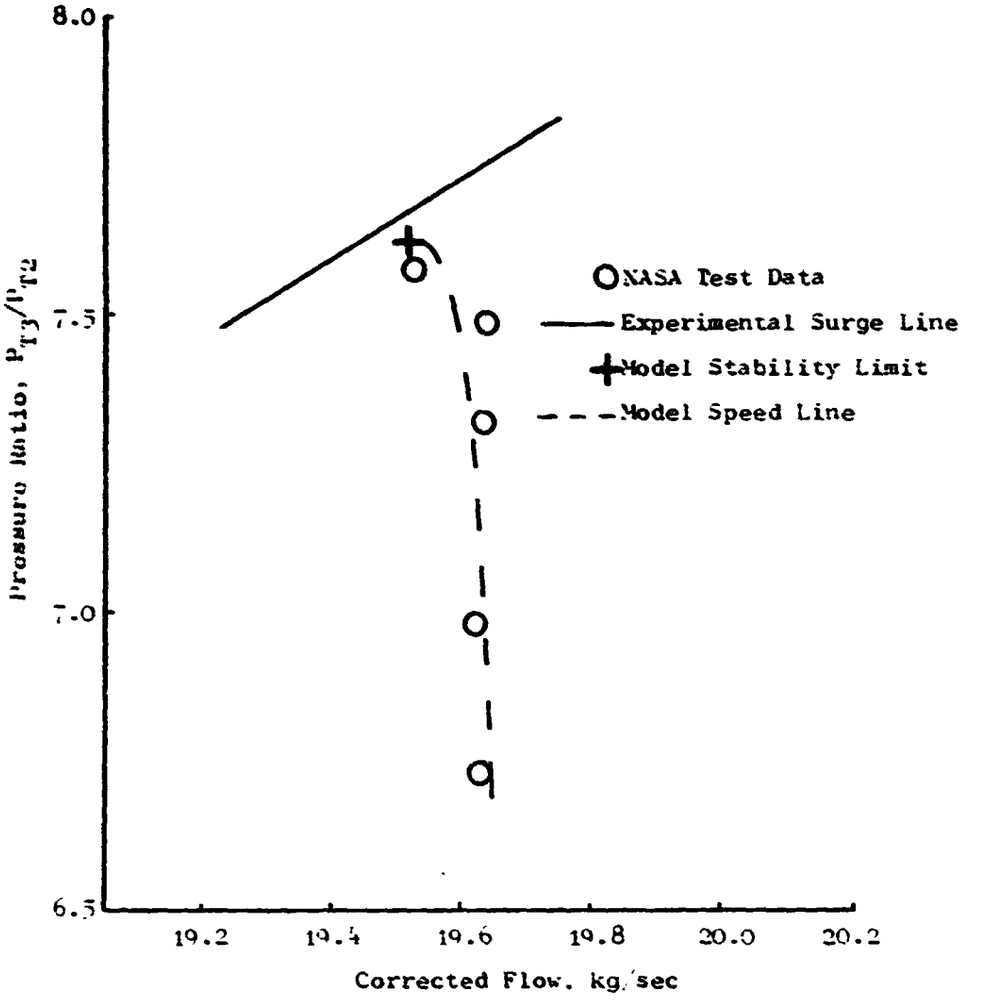

Figure 32. Clean-Inlet-Throttling Simulation, "Moss" J85-13 Engine With Stator Loss, 100% N.C.

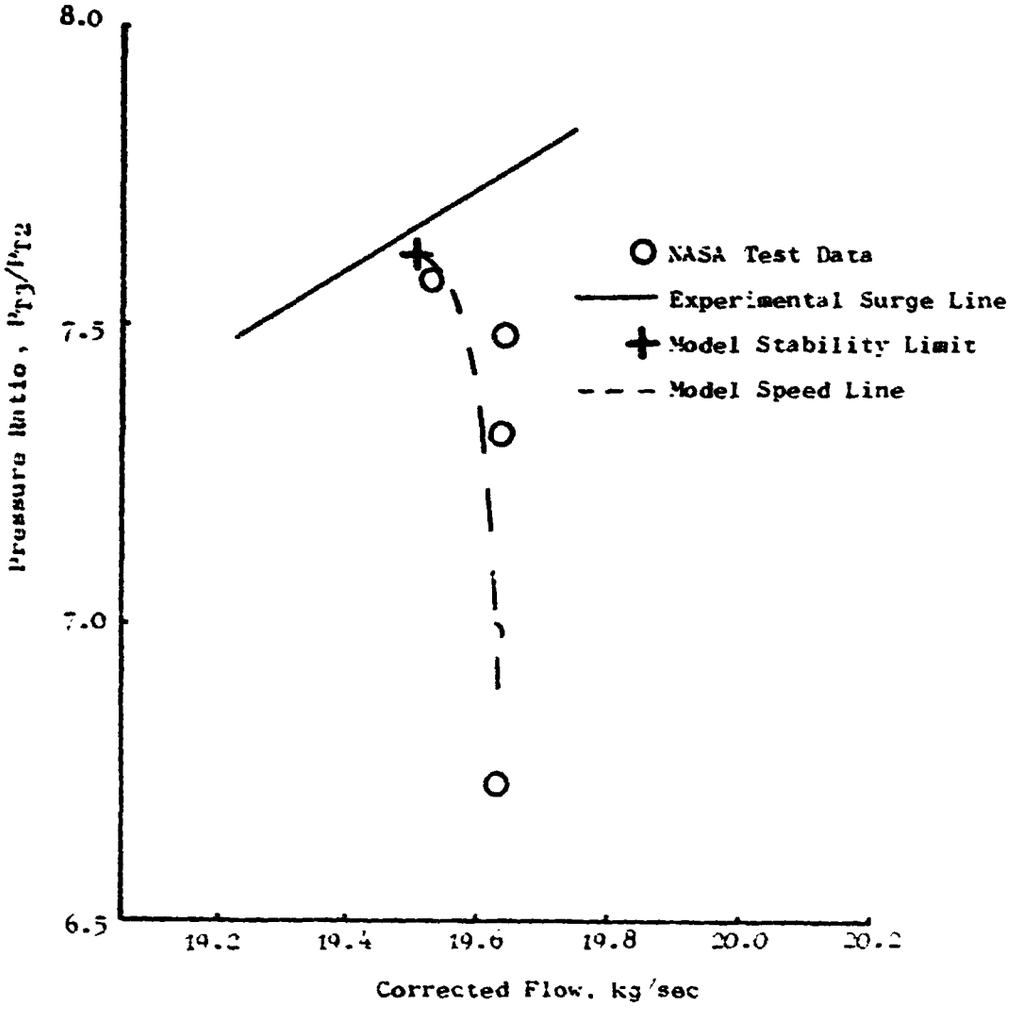

Figure 33. Clean-Inlet-Throttling Simulation, "Moss" J85-13 Engine Without Stator Loss, 100% N2.

5.0 STAGE CHARACTERISTIC SENSITIVITY STUDY

A study was made to identify the impact of measurement error on the derivation of stage characteristics and the resulting effect on the prediction of the stability limits of the compression component. This analysis was conducted using the "Moss" J85-13 engine characteristics at 80% and 100% corrected speeds. At each speed the total pressure at the exit of one stage was varied ±1% while holding the total temperature constant. The modified non-dimensional characteristics were derived with the constraint that the clean-inlet-flow overall compressor characteristics were maintained. The stage selected for the parametric variation of exit total pressure was the most aft stage in the compressor with a positive slope pressure coefficient characteristic. These stages were chosen because it was thought they might produce the largest effect on stability. At 80% corrected speed, stage 4 was selected and at 100% corrected speed, stage 3 was selected.

Figures 34 and 35 illustrate the non-dimensional characteristics for the 80% corrected speed line with and without the deviation in total pressure. Only stages 4 and 5 are shown as these are the only stages affected by a change in stage 4 exit total pressure. Similar results are shown in Figures 36 and 37 for the variation at 100% corrected speed in the stage 3 exit total pressure. Since the dynamic analysis program uses blade-row characteristics in the form of loss coefficient and deviation angle, the modified non-dimensional stage characteristics were used to generate the blade-row characteristics. Figures 38 through 41 illustrate the change in loss coefficient and deviation angle as a function of change in total pressure for the 80% and 100% corrected speed lines.

The impact of the change in characteristics on the stability limit was evaluated through a series of clean-inlet-flow throttling simulations which were performed on both the 80% and 100% corrected speed lines. Figures 42 and 43 illustrate the 80% corrected speed throttling simulations for plus and minus one percent variation of the stage 4 total pressure, respectively. The stability limit of the original simulation and the experimental surge line are shown on the figures. It can be seen that there is no significant difference between the original simulation and the total-pressure variation simulations. Similarly, Figures 44 and 45 show the 100% corrected speed throttling simulations for plus and minus one percent stage 3 exit total-pressure variation, respectively. Again the same conclusions can be drawn as for the case of the 80% corrected speed throttling simulations. Based on these analyses, it appears that the stability limit of the compressor is primarily dependent upon the shape of the overall speed line rather than the level of some of the individual stage characteristics. No change in the location of the stalling stage was observed as a result of perturbing the stage characteristics.

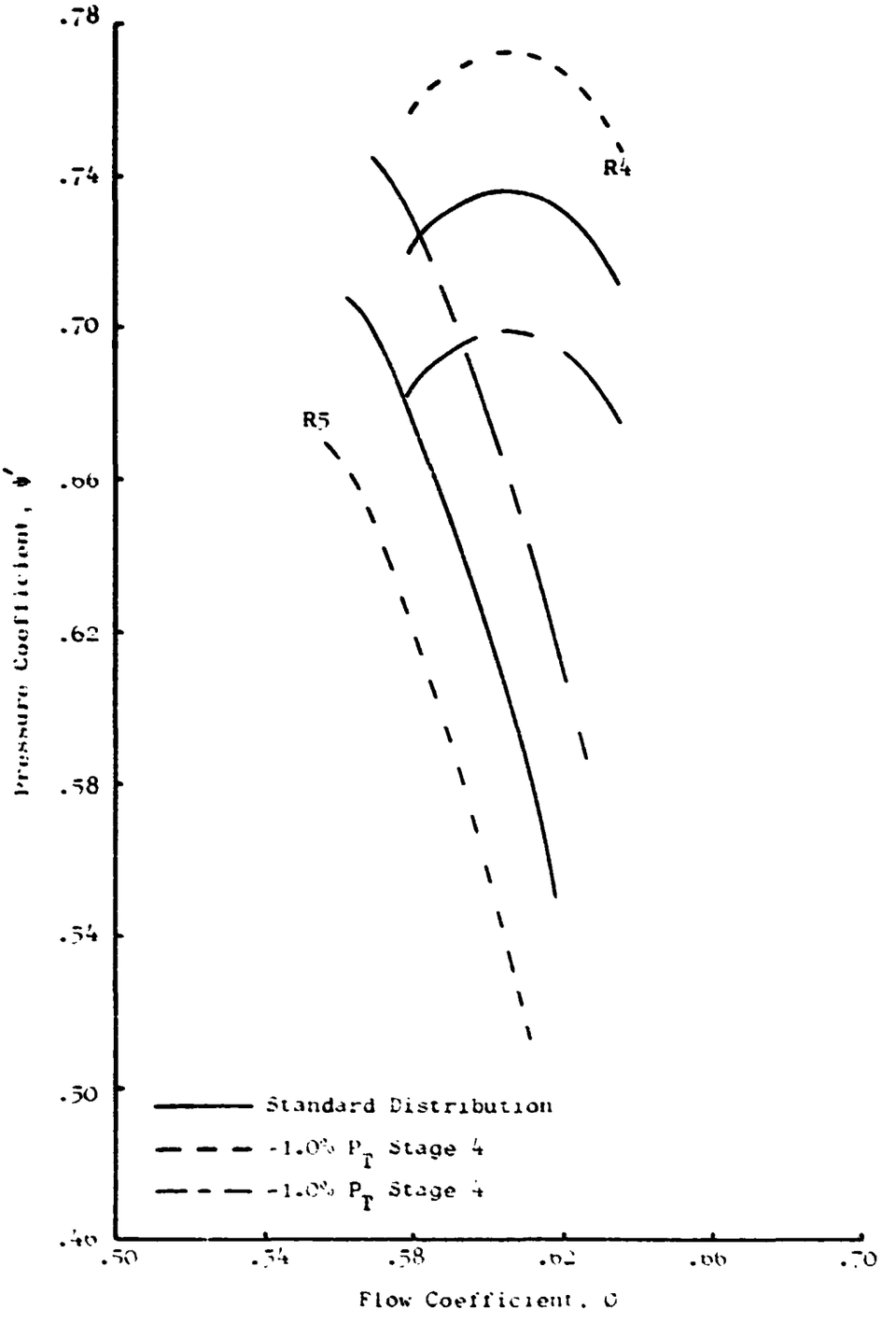

Figure 34. Pressure Coefficient Variations, "Moss" J85-13 Engine, 80% N$_2$.

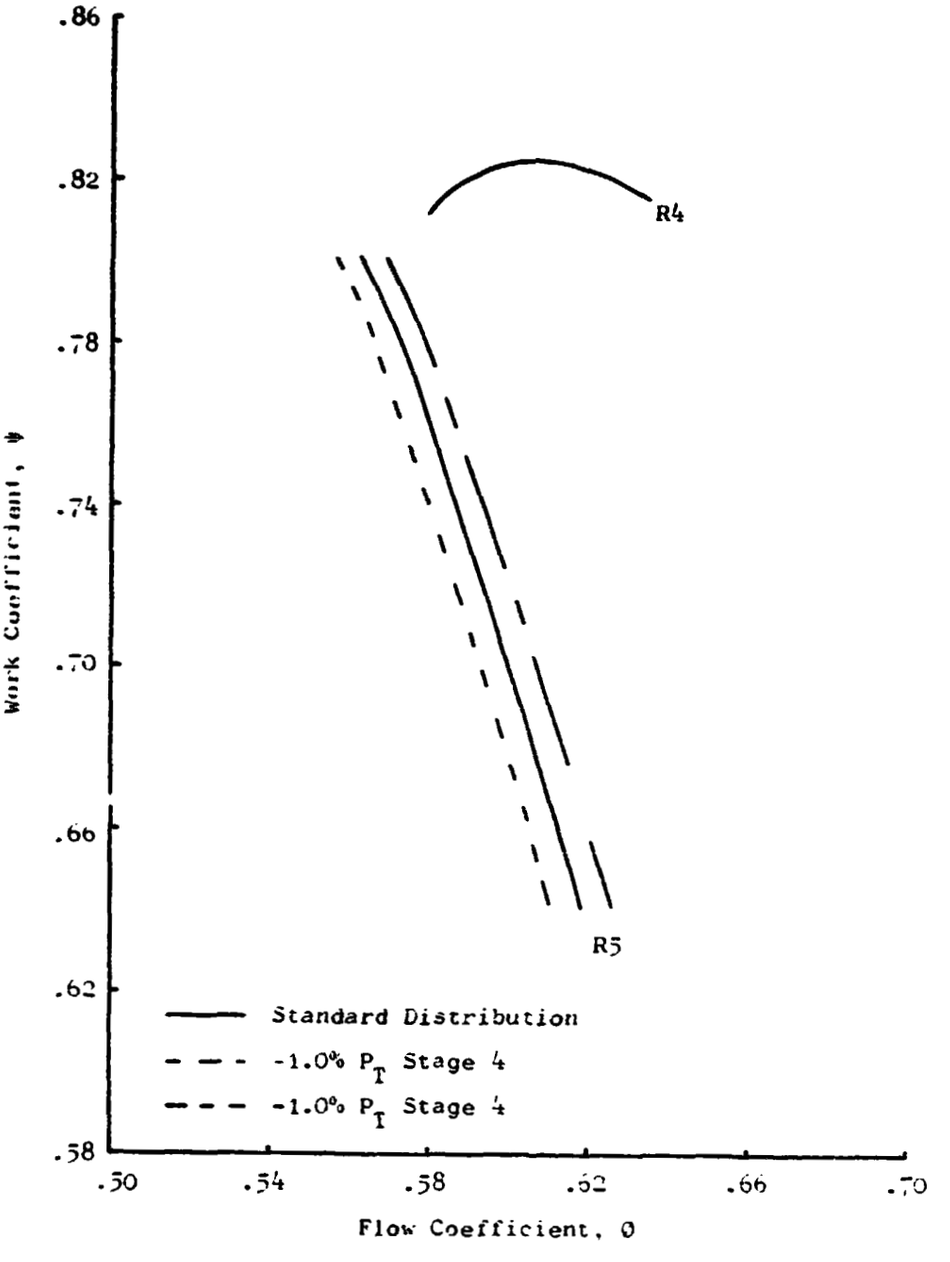

Figure 35. Work Coefficient Variations, "Moss" J85-13 Engine, 80% N.C.

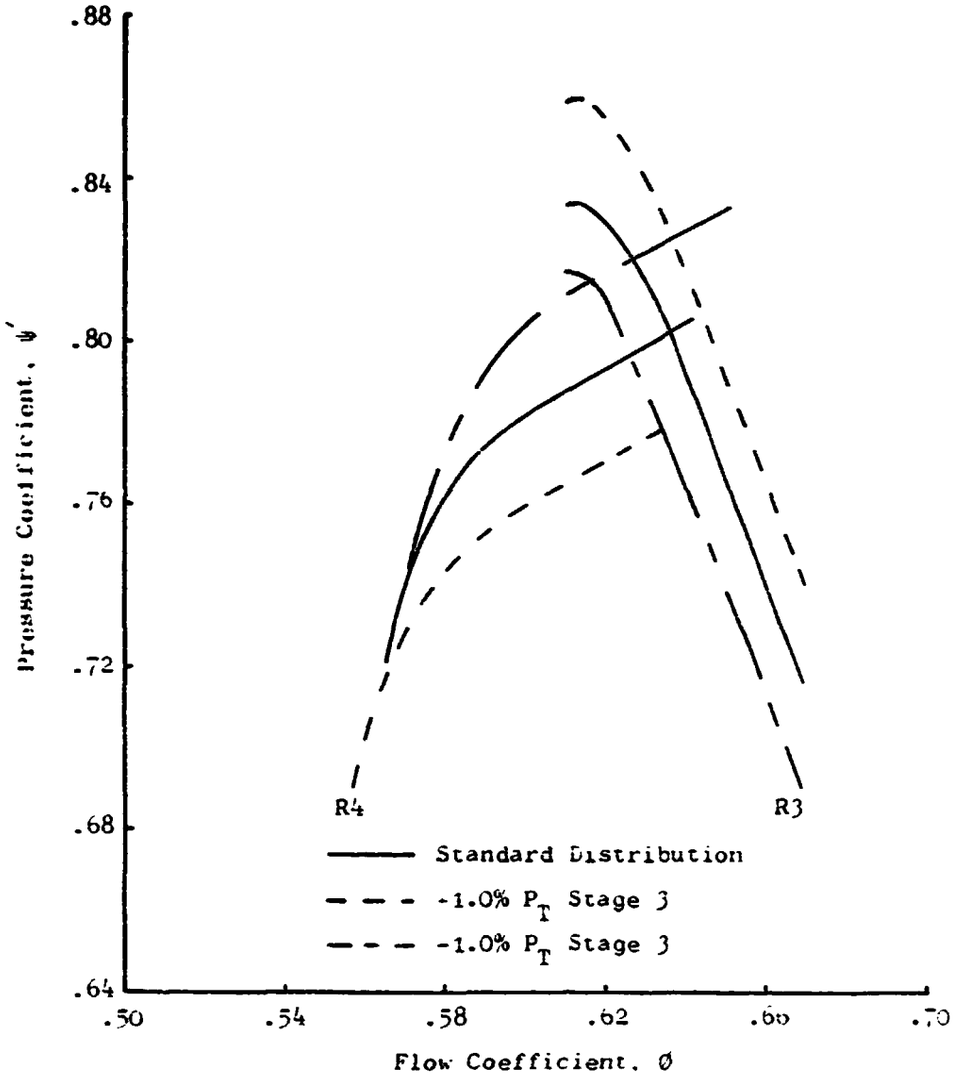

Figure 36. Pressure Coefficient Variations, "Moss" J85-13 Engine, 100% N/√θ.

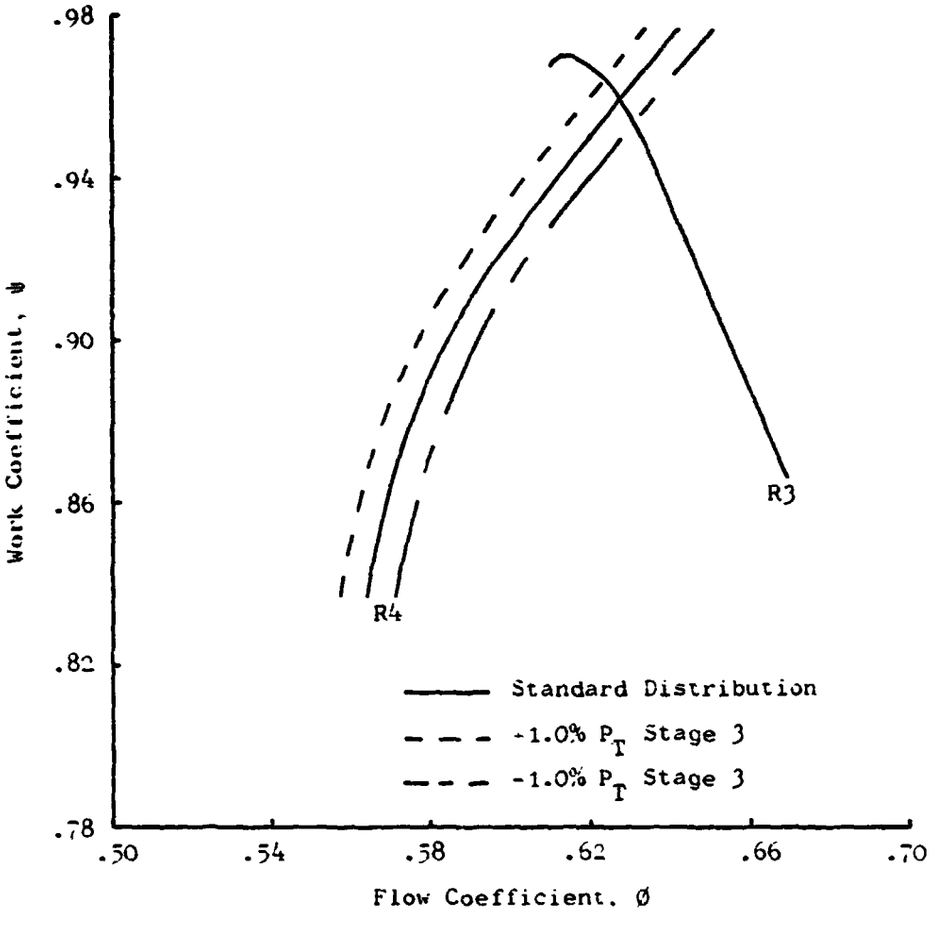

Figure 37. Work Coefficient Variations, "Moss" J85-13 Engine, 100% $N/\sqrt{\theta}$.

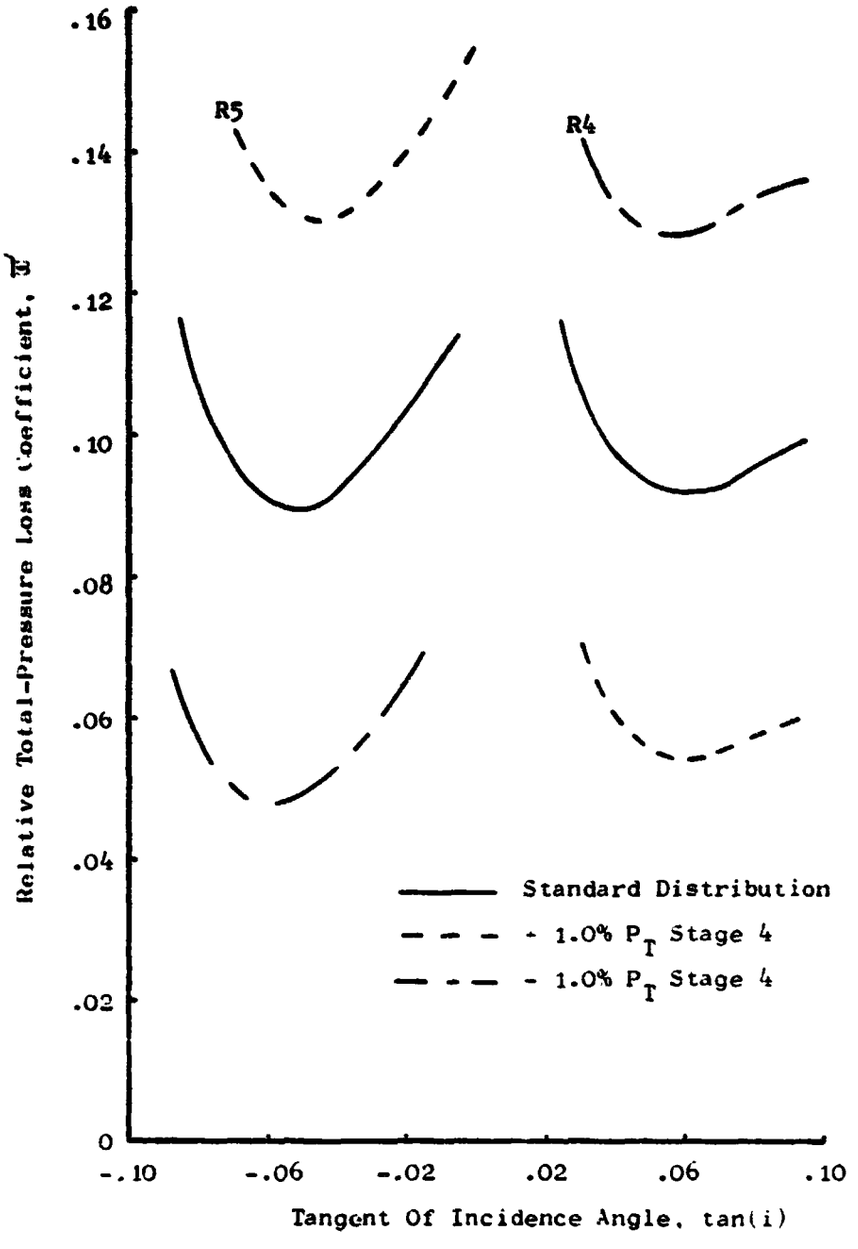

Figure 38. Relative Total-Pressure Loss Coefficient Variations, "Moss" J85-13 Engine, 80% $N/\sqrt{\theta}$.

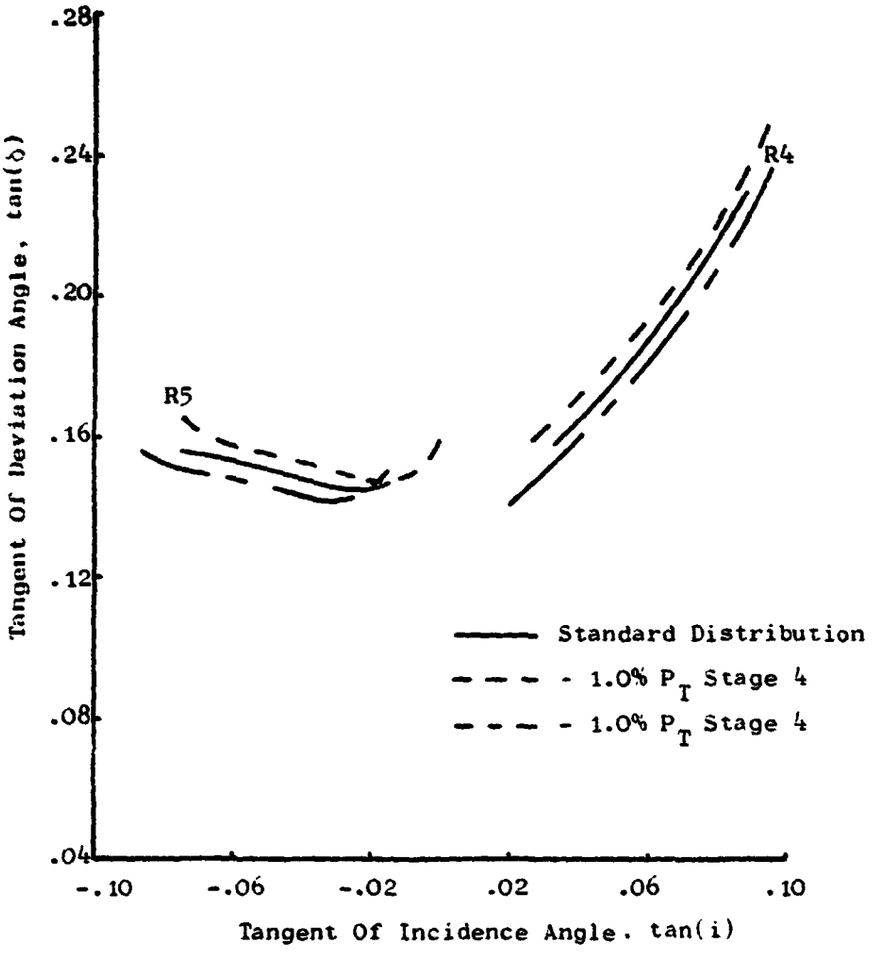

Figure 39. Tangent of Deviation Angle Variations, "Moss" J85-13 Engine, 80% $N/\sqrt{\theta}$.

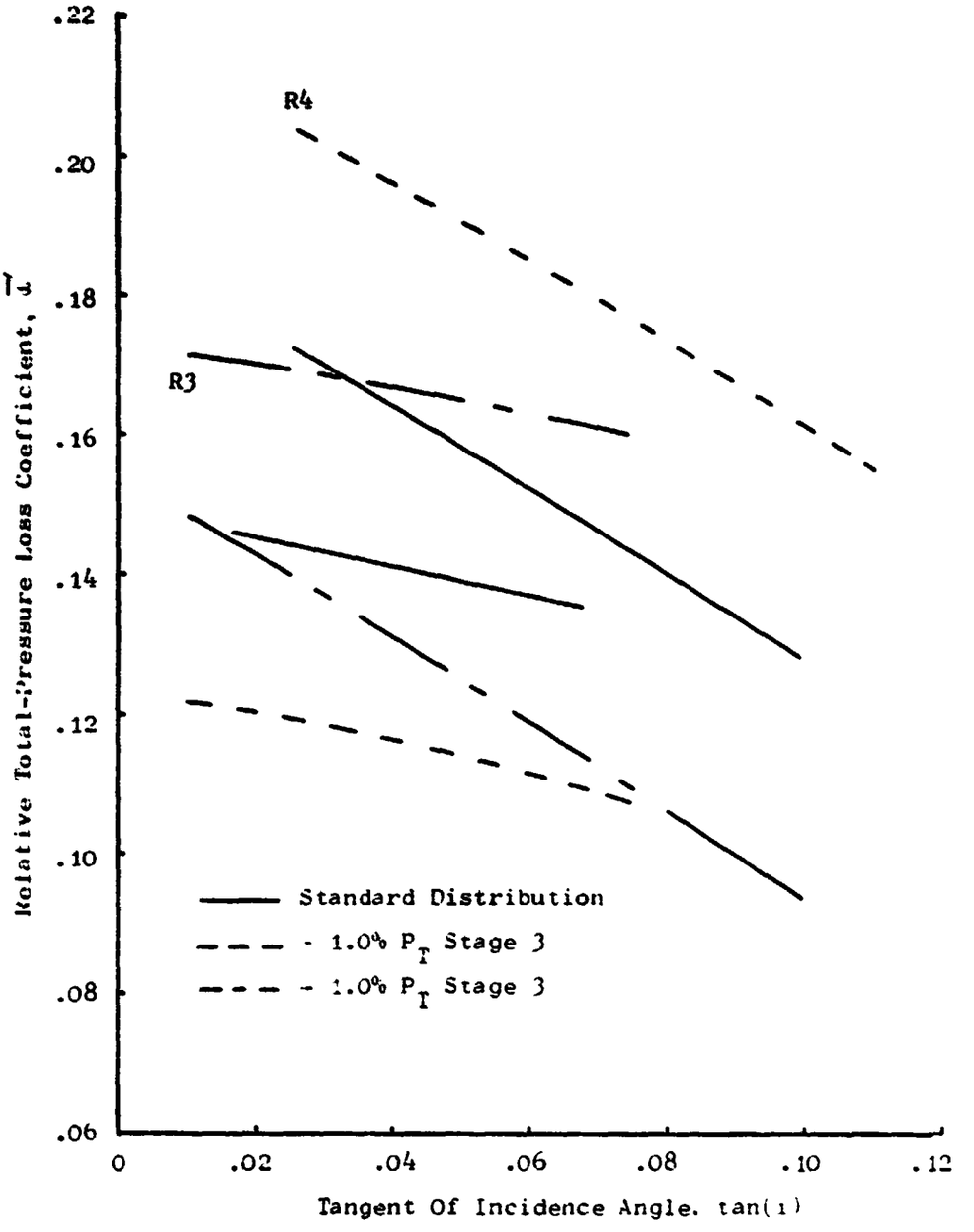

Figure 40. Relative Total-Pressure Loss Coefficient Variations, "Moss" J85-13 Engine, 100% N/√θ.

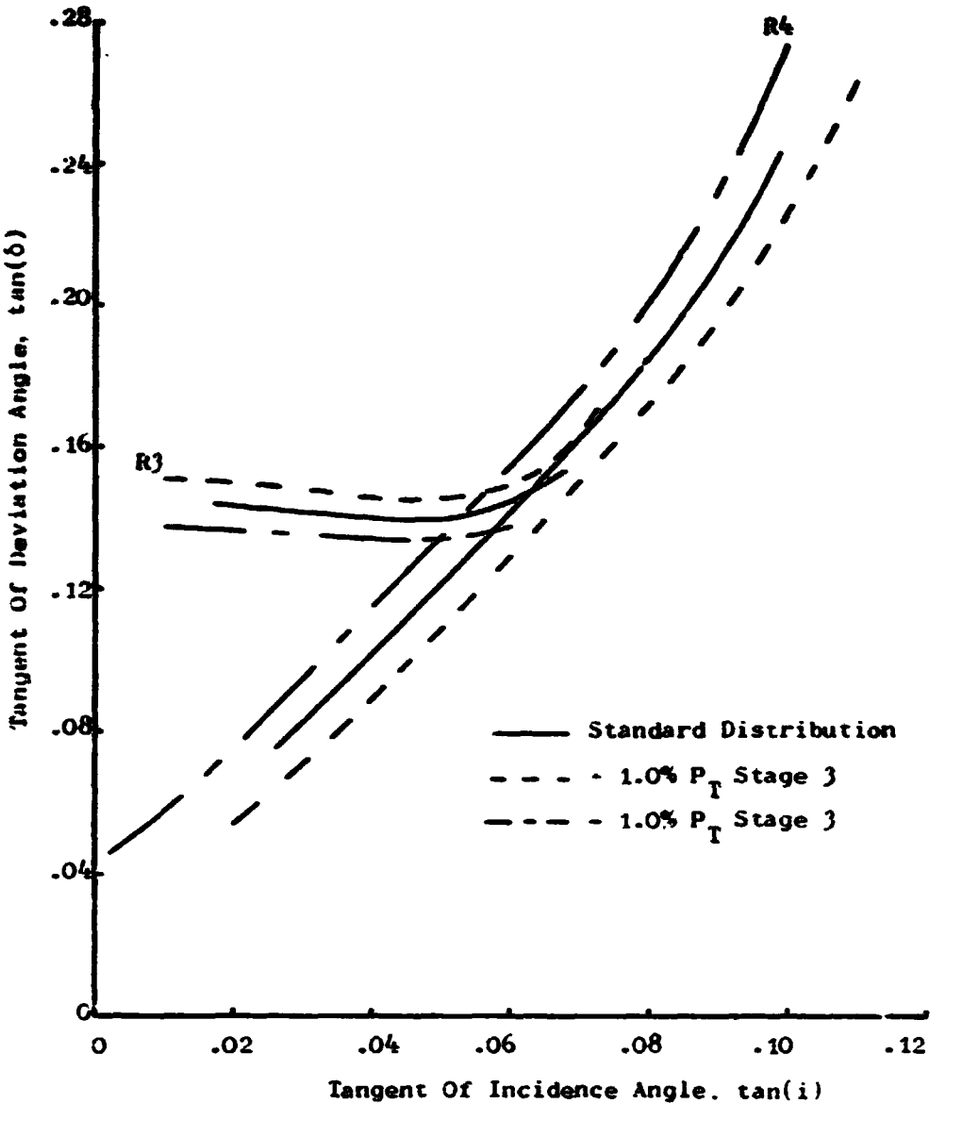

Figure 41. Tangent of Deviation Angle Variations. "Moss" J85-13 Engine, 100% N/ .

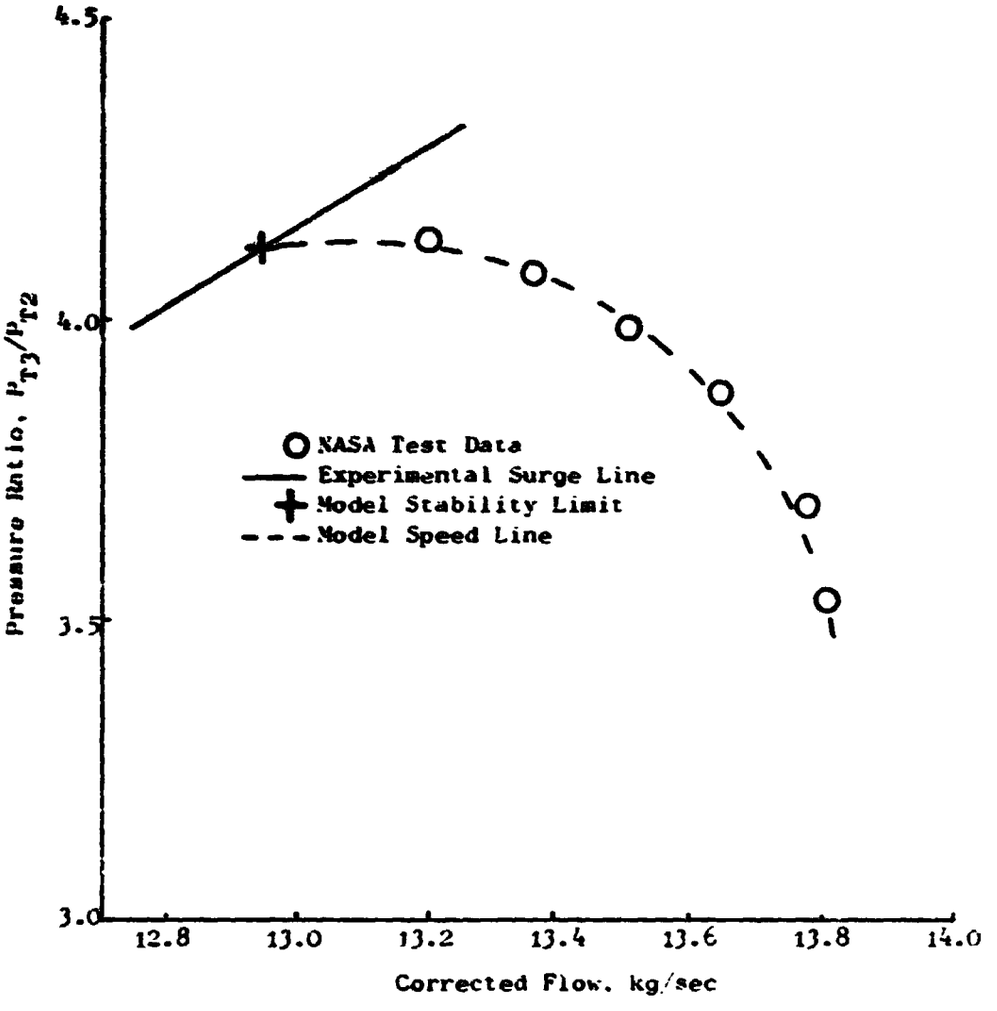

Figure 42. Clean-Inlet-Throttling Simulation, "Moss" J85-13 Engine, 80% $N/\sqrt{\theta}$, Plus One Percent Stage 4 Total-Pressure.

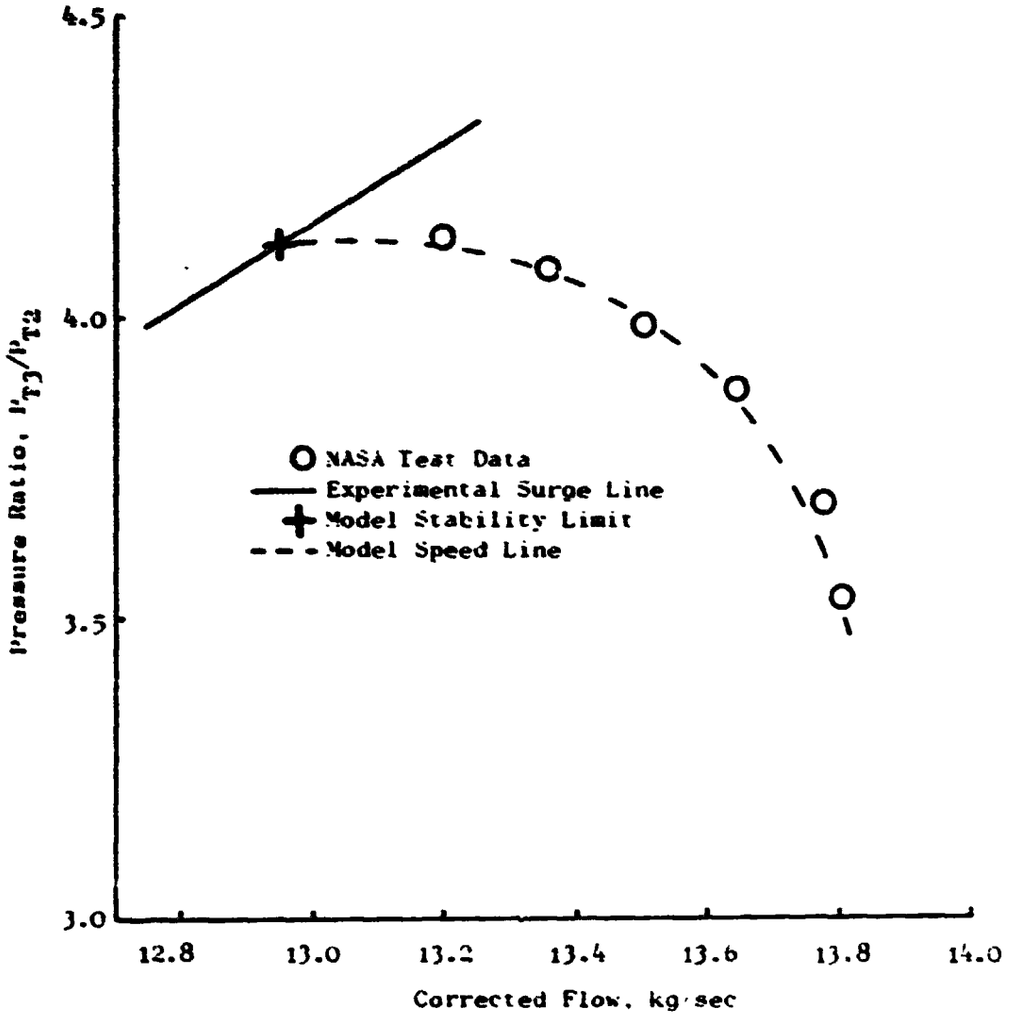

Figure 43. Clean-Inlet-Throttling Simulation, "Moss" J85-13 Engine, 80% N[illegible], Minus One Percent Stage 4 Total-Pressure.

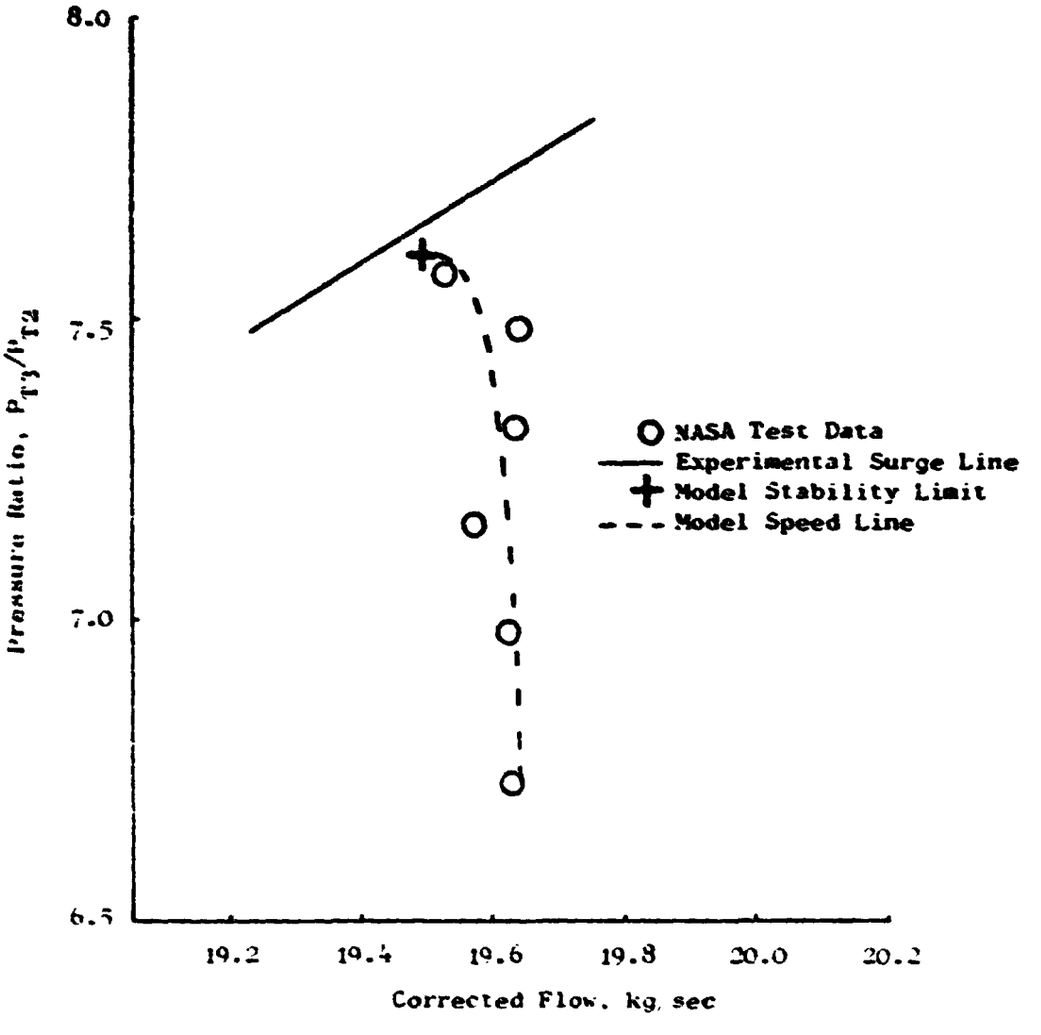

Figure 44. Clean-Inlet Throttling Simulation, "Moss" J85-13 Engine, 100% $\tilde{N}_2$, Plus One Percent Stage 3 Total-Pressure.

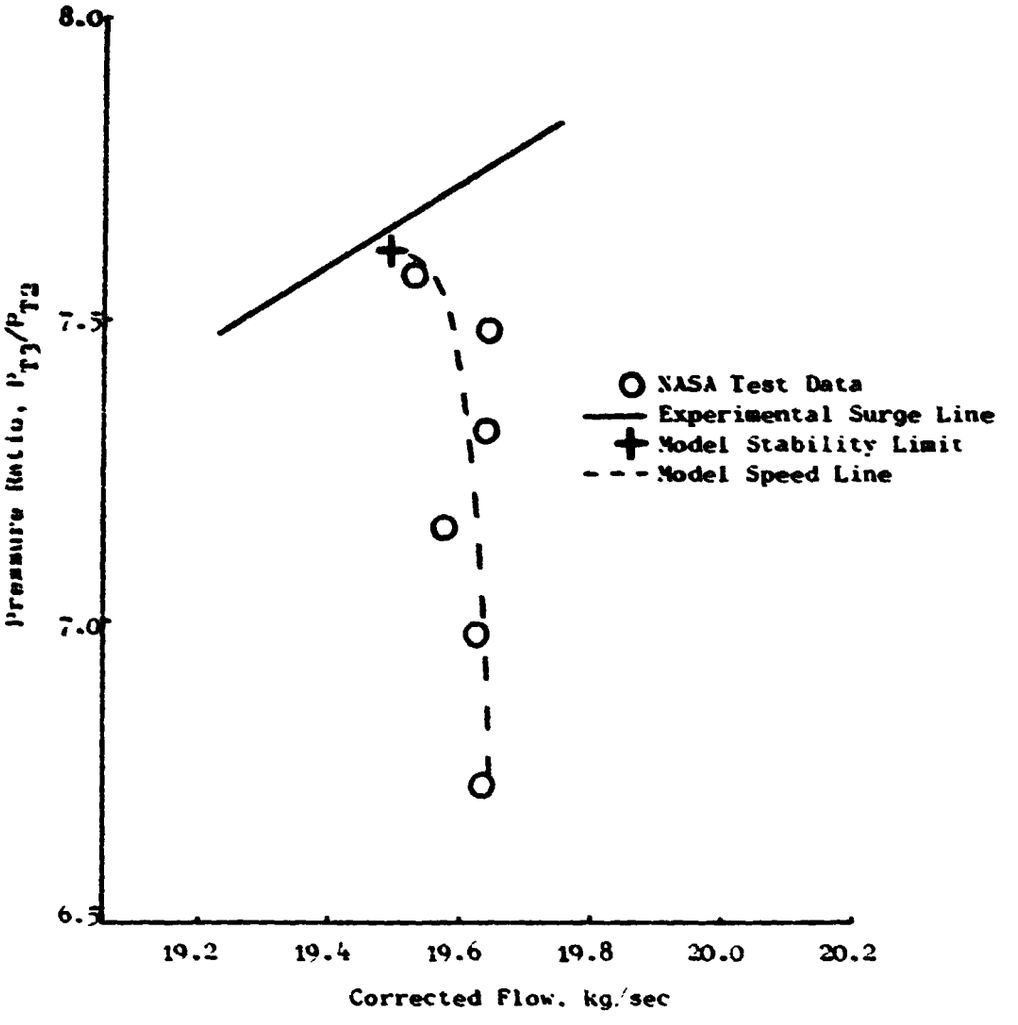

Figure 45. Clean-Inlet-Throttling Simulation, "Moss" J85-13 Engine, 100% N/$\sqrt{\theta}$, Minus One Percent Stage 3 Total-Pressure.

6.0 CONCLUSIONS AND RECOMMENDATIONS

The dynamic parallel-compressor modeling activities discussed in Reference 1 led to recommendations which seemed to offer potential for the development of greater insight into compressor modeling in general and stability modeling in particular. The activities reported upon herein include an evaluation of these recommended techniques.

The ability to calculate circumferential redistribution effects in blade-free volumes was developed and demonstrated within the computational logic of the original Dynamic Digital Blade Row Compression Component Stability Model. It is significant that gross redistribution effects for the purposes of stability calculations can be predicted without resorting to a fine mesh, differential form of the equations of change. Although the redistribution model has not materially improved the prediction capability for the J85-13, it is now recognized that the full potential of the model could not be evaluated when simulating a compressor with an IGV. A model of a fan without an IGV would be a more sensitive vehicle for evaluating the capability of the circumferential redistribution portion of the model. This effort is being accomplished as part of a yet to be published study. Further, it is recommended that other algorithms for defining sector interface values in the circumferential direction be investigated. While such schemes are conceptually simple to formulate, it is noted that they are fundamental to maintaining numerical stability, an attribute which few algorthims can maintain.

Preliminary investigations revealed that significant gains in the data-match capability of the model may be realized by approximating the response of a rotor-blade flow field to distortion. Considerably more work needs to be accomplished to establish the dependence of the rotor flow-field response to rotor geometry, speed, and possibly other unknown factors.

Inclusion of variable stator losses in the dynamic model resulted in the model becoming more responsive to the throttling boundary condition. This increased responsiveness has potential payoff in improved computational economics and more valid representations of transient events. Further, no significant difference in the predicted stability limit of the compression component with or without the inclusion of variable stator losses occurred.

An evaluation of the stage characteristic sensitivity to measurement error was performed for two speeds on the J85-13 engine and provided insight into the impact of such variations on the overall stability limit. It was shown that the stability of the compressor was established by the overall characteristics of the compressor rather than by changes in level to an individual stage. However, it is recognized that only one stage measurement was varied and it cannot be assumed that this conclusion is valid for level changes in any stage. Furthermore, the impact of isolated measurement errors or test data extrapolations which might result in a variation in stage characteristic slope were not evaluated.

REFERENCES

1. Tesch, W.A., and Steenken, W.G., "Blade Row Dynamic Digital Compressor Program, Volume 1, J85 Clean Inlet Flow and Parallel Compressor Models," National Aeronautics and Space Administration Contractor Report, CR-134979, 1976.

2. Plourde, G.A., and Stenning, A.H., "Attenuation of Circumferential Inlet Distortion in Multistage Axial Compressors," J. of Aircraft v5, n3, pp. 236-242.

3. Spring, A.H., "Upstream Influence of an Axial Compressor on Circumferentially Distorted Flow," Proceedings of the Air Force Airframe - Propulsion Compatibility Symposium, Air Force Aero Propulsion Laboratory Technical Report AFAPL-TR-69-103, June 1970.

4. Tesch, W.A., Moszee, R.H., and Steenken, W.G., "Linearized Blade Row Compression Component Model, Stability and Frequency Response Analysis of a J85-13 Compressor," National Aeronautics and Space Administration Contractor Report, CR-135162, 1976.

5. Milner, E.J., and Wenzel, L.M., "Performance of a J85-13 Compressor With Clean and Distorted Inlet Flow," National Aeronautics and Space Administration Technical Memorandum, TMX-3304.

6. Bird, R.B., Stewart, W.E., and Lightfoot, E.N., Transport Phenomena, Wiley, New York, 1960.

7. Tesch, W.A. and Doyle, V.L., "Evaluation of Range and Distortion Tolerance for High Mach Number Transonic Fan Stages, Volume I, Task II Stage Data and Performance Report for Inlet Flow Distortion Testing," National Aeronautics and Space Administration Contractor Report NASA CR-72786, 1971.

8. Reynolds, G.G., and Steenken, W.G., "Dynamic Digital Blade Row Compression Component Stability Model, Model Validation and Analysis of Planar Pressure Pulse Generator and Two-Stage Fan Test Data," Air Force Aero Propulsion Laboratory Technical Report AFAPL-TR-76-76, August 1976.

9. Kimzey, W.F., "An Analysis of the Influence of Unsteady Cascaded Airfoil Behavior on Axial Flow Compressors with Unsteady and Distorted Inflow," Paper Prepared for Tennessee Section AIAA Colloquium and Festschrift Honoring Dr. B.H. Goethert, November 1975.